理學博士學位論文

Regulation of Synapse Development and Neuronal Survival by Spartin, a Hereditary Spastic Paraplegia (HSP) Protein

유전경직성하반신마비 단백질인 Spartin 에 의한
시냅스 성장과 신경세포 생존의 조절

2013 년 8 월

서울대학교 대학원
치의과학과 신경생물학
이 민 정

Regulation of Synapse Development and Neuronal Survival by Spartin, a Hereditary Spastic Paraplegia (HSP) Protein

by

Min-Jung Lee

Advisor:

Prof. Seungbok Lee, Ph. D.

A Thesis Submitted in Partial Fulfillment of the
Requirements for the Degree of Doctor of Philosophy

June, 2013

Department of Cell and Developmental Biology
Seoul National University

ABSTRACT

Troyer syndrome is a hereditary spastic paraplegia caused by human *spartin* (*SPG20*) gene mutations. I have generated a *Drosophila* disease model showing that Spartin functions presynaptically with endocytic adaptor Eps15 to regulate synaptic growth and function. Spartin inhibits bone morphogenetic protein (BMP) signaling by promoting endocytic degradation of BMP receptor Wishful Thinking (Wit). *Drosophila* Fragile X Mental Retardation Protein (dFMRP) and Futsch/MAP1B are downstream effectors of Spartin and BMP signaling in regulating microtubule stability and synaptic growth. Loss of Spartin or elevation of BMP signaling induces age-dependent progressive defects resembling hereditary spastic paraplegias, including motor dysfunction and brain neurodegeneration. Null *spartin* phenotypes are prevented by administration of the microtubule-destabilizing drug vinblastine. Together, these results demonstrate that Spartin regulates both synaptic development and neuronal survival by controlling microtubule stability via the BMP-FMRP-Futsch pathway, suggesting that impaired regulation of microtubule stability is a core pathogenic component in Troyer syndrome.

Key words: Hereditary spastic paraplegia, Troyer syndrome, Spartin, Microtubule stability, BMP signaling, NMJ synapse, Neuronal survival

Student number: 2008-30635

CONTENTS

LIST OF FIGURES

ABREVIATIONS

BMP	Bone morphogenetic protein
Csp	Cysteine string protein
Dad	Daughters against dpp
Dlg	Discs-large
EGFR	Epidermal growth factor receptor
EJCs	Evoked excitatory junction currents
EM	Electron microscopy
EndoA	Endophilin A
Eps15	Epidermal growth factor pathway substrate 15
ESCRT-III	Endosomal sorting complexes required for transport-III
FMRP	Fragile X mental retardation protein
Gbb	Glass bottom boat
GFP	Green fluorescence protein
GluR	Glutamate receptor
HA	Hemagglutinin
H&E	Hematoxylin and eosin
HRP	Horseradish peroxidases
HSP	Hereditary spastic paraplegias
Ist1	Increased sodium tolerance 1
LD	Lipid droplets
Mad	Mothers against decapentaplegic
Med	Medea
MIT	Microtubule-interacting and trafficking molecules

MS	Multiple sclerosis
MVB	Multivesicular body
NMJ	Neuromuscular junctions
P-Mad	Phosphorylated-Mad
R-Smad	Receptor-regulated Smad
Repo	Reversed polarity
Sax	Saxophone
SC	Senescence domain
SEM	Standard error of the mean
Spin	spinster
SSR	Subsynaptic reticulum
Synj	Synaptojanin
Syt	Synaptotagmin
TEVC	Two-electrode voltage-clamp
TGF-β	Transforming growth factor-beta
TIP47	Tail-interacting protein of 47 kDa
TUNEL	Terminal deoxynucleotidyl transferase dUTP nick end labeling
Tkv	Thickveins
UAS	Upstream activating sequence
UTR	Untranslated region
VB	Vinblastine
VNC	Ventral nerve cord
Wit	Wishful Thinking

This work has been largely reproduced from an article published by Nahm, M., Lee, M., Parkinson, W., Lee, M., Kim, H., Kim, YJ., Kim, S., Cho, YS., Min, BM., Bae, YC., Broadie, K., and Lee, S. (2013). Neuron, 77, 680-695.

Figure 9 was reproduced from provided as part of collaboration by Dr. Kendal Broadie and William Parkinson (Vanderbilt University)

I. Introduction

The hereditary spastic paraplegias (HSPs) are inherited neurological disorders that are characterized primarily by progressive spasticity and weakness of the lower limbs, which result from retrograde degeneration of corticospinal tract axons. Despite the identification of forty HSP loci and twenty gene products to date, the molecular basis for most forms of HSPs remains poorly understood. A previous study in *Drosophila* have demonstrated that *spichthyin* (*spict*), the *Drosophila* homolog of the HSP gene *NIPA1* (*Nonimprinted in Prader-Willi/Angelman syndrome 1/SPG6*), regulates synaptic development by attenuating neuronal BMP signaling. Consistently, subsequent studies in mammalian cells have shown that NIPA1 and two more HSP proteins, Spastin (SPG4) and Spartin (SPG20), act as inhibitors of BMP signaling, suggesting that elevated BMP signaling could be a common pathological component of at least several HSPs. In this thesis, I have sought to test this hypothesis by analyzing BMP-dependent synaptic development and neurodegeneration in *Drosophila spartin* mutants.

1. Retrograde Bone Morphogenetic Protein (BMP) Signaling in Synapse Development

Trans-synaptic retrograde signaling from postsynaptic target cells to presynaptic terminals plays critical roles in synapse formation, growth and plasticity, as well as presynaptic neuronal survival (Regehr *et al*., 2009; Zweifel *et al*., 2005). In *Drosophila*, the BMP retrograde signal Glass bottom boat (Gbb) secreted from postsynaptic muscles acts on type II receptor Wishful Thinking

(Wit) and type I receptors Thickveins (Tkv) and Saxophone (Sax) on presynaptic terminals to regulate proper growth and function of neuromuscular junction (NMJ) synapses (Aberle *et al*., 2002; Marques *et al*., 2002; McCabe *et al*., 2003; Rawson *et al*., 2003). Upon Gbb binding, two type I and two type II receptors form a tetrameric complex, which phosphorylates the Smad transcription factor Mothers against decapentaplegic (Mad). P-Mad then makes complexes with the co-Smad Medea (Med) to enter the nucleus and regulate transcription.

Drosophila NMJ studies have shown that BMP signaling is tightly regulated at multiple levels. Postsynaptic Gbb secretion is negatively regulated by the Cdc42-Wsp pathway (Nahm *et al*., 2010a; Nahm *et al*., 2010b) and presynaptic signaling is attenuated by endocytic proteins regulating internalization and endosomal trafficking of BMP receptors (O'Connor-*Giles et al*., 2008; Sweeney and Davis, 2002; Wang *et al*., 2007). Interestingly, regulators of BMP receptor endocytosis and trafficking include *Drosophila* homologs of human proteins associated with neurodegenerative diseases (Bayat *et al*., 2011), including hereditary spastic paraplegia 6 (HSP6) (Wang *et al*., 2007) and multiple sclerosis (MS) (Kim *et al*., 2010). However, the mechanisms by which elevated BMP signaling causes neuronal degeneration remain largely speculative.

2. Troyer Syndrome, Is an Autosomal Recessive Form of Hereditary Spastic Paraplegia that Is Caused by Loss-of-Function Mutations in the *spartin* Gene (*SPG20*)

HSPs comprise a heterogeneous group of neurodegenerative diseases characterized by progressive lower limb spasticity and weakness (Blackstone *et*

al., 2011). These neuropathies are due to distal degeneration of corticospinal tract axons. Troyer syndrome is an autosomal recessive, complicated HSP characterized by dysarthria, mental retardation, distal muscle wasting and short stature, in addition to lower extremity spastic weakness (Cross and McKusick, 1967). Troyer syndrome HSP is caused by loss-of-function mutations in the human spartin gene (SPG20) (Manzini *et al*., 2010; Patel *et al*., 2002), which encodes a protein consisting of several domains: an N-terminal MIT (contained in microtubule-interacting and trafficking molecules) domain, a central Eps15-interacting domain, and a C-terminal senescence domain (Bakowska *et al*., 2005; Ciccarelli *et al*., 2003).

Studies on cultured mammalian cells have shown that Spartin is a multifunctional protein in several subcellular compartments. Spartin interacts with endocytic trafficking protein Eps15 and plays a role in intracellular trafficking of epidermal growth factor receptor (EGFR), transiently localizing to endosomes upon EGF stimulation (Bakowska *et al*., 2007). Spartin also localizes transiently to midbodies during cell division through interaction with increased sodium tolerance 1 (Ist1), a component of endosomal sorting complexes required for transport (ESCRT)-III complex (Renvoise *et al*., 2010). Moreover, Spartin associates with lipid droplets (LDs) in cells treated with oleic acid and regulate their turnover, possibly by recruiting ubiquitin E3 ligases of the Nedd4 family (Eastman *et al*., 2009; Edwards *et al*., 2009; Hooper *et al*., 2010). Spartin also associates with mitochondria via interaction with cardiolipin, a phospholipid of the outer membrane, and regulates mitochondrial Ca2+ homeostasis (Joshi and Bakowska, 2011). However, it remains unclear whether these Spartin activities are involved in neuronal function and maintenance *in vivo*.

3. The *Drosophila* Neuromuscular Junction (NMJ) and Adult Brain

To study the synaptic function of Spartin and to model the pathogenesis of Troyer syndrome, I have analyzed the loss-of-function phenotypes at the *Drosophila* larval neuromuscular junctions (NMJ) and the adult brains. The larval NMJ is a glutamatergic excitatory synapse and synaptic components (neurotransmitter release machinery, glutamate receptors, and etc.) and regulatory mechanisms are highly conserved with those of vertebrates (Bellen *et al*., 2010; Broadie and Bate, 1993; Keshishian *et al*., 1994; Ryan and Grant, 2009). The axons of motor neurons extend their branches to the target muscles and form synaptic boutons, surrounded by the subsynaptic reticulum (SSR) driven by postsynaptic muscle membrane. During relatively short developmental periods, the muscle cells grow about 100 fold in size, and the number of synaptic boutons is increased (Ruiz-Canada and Budnik, 2006; Schuster *et al*., 1996). Furthermore, the NMJs are accessible to electrophysiological technique, FM dye uptake, and Ca^{2+} imaging for functional studies of the synapse. Immunohistochemistry, fluorescence microscopy, and electron microscopy provide a clear view of the synaptic structure and molecular anatomy of the synapse. In addition to the benefits of generating various mutants and transgenic flies for rescue experiments or gain of function studies, lots of genetic tools support the ability to control gene expression in a tissue-specific manner. Adult flies also exhibit complex behaviors including learning, memory and motor ability and like humans, these behaviors deteriorate with age-dependent (Mockett *et al*., 2003; Simon *et al*., 2006).

Furthermore, fly adult brains are easily accessible to study neurodegeneration. For example, hematoxylin and eosin (H&E) staining in adult brain clearly displays vacuole formation generated by neurodegeneration.

Thus, the *Drosophila* NMJs and the adult brains are one of the useful model systems to study the regulatory mechanisms of synaptic functions and to model the pathogenesis of motor neuron diseases.

4. Rationale and Outline of the Thesis Experiments

HSPs comprise a heterogeneous group of neurodegenerative diseases that are characterized by progressive spasticity and weakness of the lower limbs. To date, more than 40 genetic loci have been mapped for HSPs, and 20 spastic paraplegia genes (*SPGs*) are identified. These SPGs can be divided into several groups based on probable cellular pathogenesis. Nevertheless, the mutations in the different human HSP genes cause clinically similar disorders. These facts suggest that there should be a common pathogenic component of the HSPs.

The vertebrate and invertebrate models have recently identified the association between BMP pathway and motor neuron diseases including HSPs, Multiple Sclerosis (MS), Spinal Muscular Atrophy (SMA) and Huntington's disease. Previous studies provide compelling evidence that the endosomal groups of HSP proteins include NIPA1, Spastin and Spartin are inhibitors of mammalian BMP signaling. However, the potential connections between HSPs and elevated BMP signaling have not been known. The mutations in the human *spartin* (*SPG20*) gene cause Troyer syndrome, an autosomal recessive form of HSPs. Although the data obtained from cultured cells suggest a role for Spartin in endocytosis of plasma membrane receptors, it is unclear whether impaired endocytosis triggers the pathogenesis of Troyer syndrome HSPs. Here, I generate a *Drosophila* model system to investigate the physiological functions of Spartin and uncover the core pathogenic mechanisms of HSPs.

I show that Spartin is enriched presynaptically at the NMJ and involved in both synaptic growth and endocytosis regulation through interaction with Eps15. I further demonstrate that Spartin inhibits the retrograde BMP signaling by promoting the endocytic internalization and subsequent endosomal trafficking of the type II BMP receptor, Wit. I also provide evidence that Spartin-mediated regulation of BMP-dFMRP-Futsch signaling modulates neuronal microtubule stability, which in turn controls synaptic growth and neuronal survival. This study suggests that the impaired regulation of microtubule stability is a core pathogenic component in HSPs.

II. Materials and Methods

1. *Drosophila* Stocks and Transgenes

The w^{1118} strain was used as the wildtype control. An *EP* insertion in the *spartin* locus (G8635) was obtained from GenExel (Republic of Korea) and imprecisely excised to produce $spartin^{1}$. I generated transgenic lines carrying *UAS-HA-spartin*, *UAS-HA-spartinΔEps15*, and *UAS-Myc-spartin-human* in the w^{1118} background by standard procedures (Robertson *et al*., 1988). *Df(3R)110* (a deficiency uncovering the *spartin* locus), wit^{A12}, wit^{B11}, mad^{237}, dad^{J1e4}, $dap160^{\Delta 1}$, $endo^{\Delta 4}$, $synj^{1}$, $dfmr1^{\Delta 50}$, and $futsch^{K68}$ were obtained from the Bloomington Stock Center; gbb^{1} and *UAS-gbb* from Kristi Wharton (Brown University); $eps15^{e75}$ and $eps15^{\Delta 29}$ from Hugo Bellen (Baylor College of Medicine); *UAS-GFP-myc-2xFYVE* from Marcos Gonzalez-Gaitan (University of Geneva); *UAS-wit* from Michael O'Connor (University of Minnesota); and $UAS\text{-}tkv^{CA}$ from Takashi Adachi-Yamada (Kobe University, Japan). I also used the following GAL4 lines: *C155-GAL4* (Lin and Goodman, 1994), *elav-GeneSwitch-GAL4* (*elav-GS-GAL4*) (Osterwalder *et al*., 2001), and *BG57-GAL4* (Budnik *et al*., 1996).

Flies were maintained on standard medium at 25°C unless otherwise stated. For pharmacological manipulation of microtubule stability, animals were grown on standard food containing vinblastine sulfate (Sigma). Concentrations ranging from 0.1 mM to 5 mM were tested. I used the lowest concentration (1 mM) that restores the levels of axonal Ac-Tubulin and Futsch staining close to wildtype. At this concentration, vinblastine administration did not show obvious effects on the viability, fertility, NMJ morphology, adult brain

architecture of wildtype animals. For the experiments presented, newly eclosed adult flies grown in the absence of vinblastine were transferred to vinblastine-containing food for aging.

2. Molecular Biology

Plasmid construction, RT-PCR, and quantitative real-time PCR were performed according to standard protocols. Full-length cDNAs for *Drosophila spartin* and *wit* were obtained from the *Drosophila* Genomics Resource Center (clone ID: HL01040 and GH13548, respectively). The cDNA insert was subcloned into pcDNA3.1 (+)-HA (Invitrogen) to generate *pcDNA-HA-spartin*. I also generated *pcDNA-HA-spartinΔEps15* via PCR-based mutagenesis. Full-length cDNA for human *spartin* was amplified by reverse transcription PCR (RT-PCR) of mRNA prepared from HEK293 cells and inserted into pCMV-Tag3B (Stratagene) to generate *pCMV-Myc-spartin-human*. For transgenic rescue experiments, the *HA-spartin* and *Myc-spartin-human* cDNA sequences were introduced into pUAST (Brand and Perrimon, 1993) to produce *UAS-HA-spartin, UAS-HA-spartinΔEps15*, and *UAS-Myc-spartin-human*. For expression in bacteria or S2R+ cells, *spartin* cDNA fragments of interest were amplified by PCR and subcloned into either the pGEX6P1 (Amersham Pharmacia) or pAc5.1 (Invitrogen) vector, respectively.

To assess the effect of the *spartin*^{1} mutation on the expression levels of *spartin* and its neighboring gene *Karyb3*, total RNA extracted from larvae was reverse-transcribed into cDNA as described previously (Nahm *et al*., 2010b). cDNAs were analyzed by PCR using the following primers: *spartin*, 5'-TCGCTGGCACGGTAGTGCAGC'-3 and 5' CGTATTCGATGGCCTCGAGAC-3'; *Karyb3*, 5'-

CGTTTGGCGGCTCGCAATGAG-3’ and 5’-ACAGAGAATGCGATCTCGGCG-3’; and *rp49*, 5’-CACCAGTCGGATCGATATGC-3’ and 5’-CACGTTGTGCACCAGGAACT-3’. Expression of *rp49* was used as an internal control.

To determine whether levels of *dfmr1* RNA are influenced by Spartin and BMP signaling, total RNA extracted from the larval CNS was reverse-transcribed into cDNA. cDNAs were analyzed by quantitative real-time PCR (qRT-PCR) using Applied Biosystems SYBR Green PCR Mater Mix on an Applied Biosystems 7500 Real-Time PCR machine. The following primers for *dfmr1* were used in this study: 5'-GGA TCA GAA CAT ACC ACG TG-3' and 5'-CGC CTC CAC GAT AGC TGC CAG-3'. Expression of *rp49* was used as an internal control. Relative quantification was performed using the comparative CT method (ABI manual).

3. Cell Culture and Double-Stranded RNA Interference

Drosophila Schneider S2R+ cells were maintained at 25°C in Schneider’s medium (Invitrogen) supplemented with 10% heat-inactivated fetal bovine serum (FBS). Double-stranded RNA interference (dsRNAi) was carried out in six-well culture plates containing 2 X 10^6 S2R+ cells as described previously (Lee *et al*., 2007). *Spartin* dsRNA was generated by *in vitro* transcription of a DNA template containing T7 promoter sequences at both ends. The DNA template was generated by PCR using the primers containing a T7 promotor sequence upstream of the following *spartin*-specific sequences: 5’-TCGTCAACTATGTCATTGGTAA-3’ and 5’-GCGTCATCTTGGAAATGATATA-3’.

4. Generation of Anti-Spartin Antibody and Western Blot Analysis

A rat polyclonal antibody against Spartin was generated against a purified GST fusion containing amino acids 102-292 of Spartin. Antisera were affinity purified using the same recombinant protein cross-linked CNBr-activated Sepharose 4 Fast Flow beads (GE Healthcare). Western blot analyses were performed as described previously (Nahm *et al*., 2010b). The third instar larvae and adult heads were washed twice in ice-cold PBS and mixed with 1X SDS sample buffer. After boiling for 5 minutes, the homogenates were subjected to SDS-PAGE. Gels were transferred onto nitrocellulose membranes (Whatman) and blocked with 5 % bovine serum albumin (BSA). Primary antibody was incubated for overnight at 4 °C. Blots were detected with an ECL detection system (Fierce). The following antibodies were used in this study: anti-Spartin (Roche, 1:1000), anti-pMad (Cell Signaling, 1:1000), anti-acetylated α-Tubulin (Sigma, 1:500), anti-Futsch (22C10, Developmental Studies Hybridoma Bank, 1:500) and HRP-conjugated secondary antibody (Jackson ImmunoResearch, 1:4000).

5. Immunohistochemistry and Imaging of Larval NMJs

Wandering third-instar larvae were dissected in Ca^{2+}-free HL3 saline (Stewart *et al*., 1994) and fixed in PBS containing 4% formaldehyde for 30 min. Fixed preparations were washed with PBT-0.1 (PBS, 0.1% Triton X-100), blocked with 5% BSA/PBT-0.1 for 1 hr, and incubated with primary antibodies as described previously (Nahm *et al*., 2010a). I used the following primary antibodies: FITC-conjugated anti-HRP (Jackson ImmunoResearch laboratories) at 1:200, anti-P-Mad (PS1) (Persson *et al*., 1998) at 1:100, anti-α-Tubulin and

anti-acetylated α-Tubulin (Sigma) at 1:500, anti-tyrosinated α-Tubulin (Chemicon) at 1:40, anti-Rab5 (Abcam) at 1:100, and anti-GFP (Millipore) at 1:100. The following antibodies purchased from the Iowa Developmental Studies Hybridoma Bank were also used: anti-Bruchpilot (nc82) at 1:10, anti-Futsch (22C10) at 1:50, anti-Wit (23C7) at 1:100, and anti-Synaptotagmin 1 (3H2 2D7) at 1:5. FITC-, Cy3- and Cy5-conjugated secondary antibodies (Jackson ImmunoResearch Laboratories) were used at 1:200.

Fluorescence images of NMJs labeled with anti-HRP were acquired with a FV300 laser-scanning confocal microscope (Olympus) and accompanying FLOUVIEW software using a Plan Apo 40× 0.90 NA or U Plan Apo 100× 1.3 NA objective. Other fluorescence images were acquired with a LSM 700 laser-scanning confocal microscope (Carl Zeiss) with the ZEN imaging software using a C-Apo 40× 1.20 W or Plan- Apo 100× 1.40 oil objective. For comparison between different genotypes, samples were processed simultaneously and imaged under identical confocal settings. All quantifications were performed at NMJ 6/7 in A2 segment. In the analysis of NMJ morphology and levels of P-Mad, confocal sections were maximally projected. Quantification of bouton number and satellite bouton number was performed as previously described (Nahm *et al*., 2010a).

6. Electrophysiology and FM1-43 Uptake Assays

Two-electrode voltage-clamp (TEVC) electrophysiology recordings was performed at 18°C on the wandering third instar NMJ, as reported previously (Rohrbough *et al*., 1999; Verstreken *et al*., 2008). Staged larvae were glued with 3M Vetbond tissue adhesive to a sylgard-coated glass coverslip, cut longitudinally along the dorsal midline, internal organs removed and the

sides glued down to allow access to the neuromusculature. The nerves were then cut close to the ventral nerve cord (VNC) with a pair of fine scissors. Dissections and recordings were performed in bath saline consisting of 128 mM NaCl, 2 mM KCl, 4 mM $MgCl_2$, 1.0 mM $CaCl_2$, 70 mM sucrose, 5 mM trehalose, and 5 mM HEPES, pH 7.1. Preparations were imaged using a Zeiss Axioskop microscope with a 40X water immersion objective. A fire-polished glass suction electrode containing saline was used for evoked nerve stimulation of the severed motor nerve with a 0.5-msec supra-threshold stimulus at 0.2 Hz from a Grass S88 stimulator. Muscle 6 in abdominal segments 2 or 3 was impaled with two microelectrodes of ~15 MΩ resistance filled with 3 M KCl. The muscle was clamped at -60 mV using an Axoclamp-2B TEVC amplifier. Evoked excitatory junctional current (EJC) records were filtered at 2 kHz. Spontaneous miniature EJC (mEJC) records were made in 2-min sessions filtered at 0.5 kHz. The JMP10 software was used for statistical comparisons with Tukey-Kramer tests unless indicated. The sample size was $n \geq 10$ animals for each genotype. This experimentation was provided as part of collaboration with Dr. Kendal Broadie and William Parkinson (Vanderbilt University).

For FM1-43FX dye uptake experiments, wandering third instar larvae were dissected in Ca^{2+}-free HL3 saline. The preparation was washed with fresh HL3 saline and then incubated in HL3 containing 90 mM KCl, 5 mM $CaCl_2$, and 4 mM FM1-43FX dye (Molecular Probes). After dye loading, the samples were washed for 10 min in HL3 saline without Ca^{2+} and then fixed in 4% formaldehyde in PBS for 30 min, followed by washing with PBS three times. Images were acquired using an FV300 laser-scanning confocal microscope (Olympus) using a Plan Apo 60x 1.4 NA Oil objective. The fluorescence intensity was measured using the FLOUVIEW software.

7. Histology, Immunostaining, and TUNEL Staining of Adult Brains

For the assessment of neurodegeneration in adult brains, H&E staining on paraffin sections and immunostaining and TUNEL staining on cryosections were performed according to standard protocols. Paraffin sectioning and H&E staining of adult brains were performed as described previously (Drobysheva *et al*., 2008). Briefly, heads from were removed and fixed overnight in 4% formaldehyde in PBS. Paraffin-embedded brains were subjected to serial 5-μm sectioning on a RM2255 microtome (Leica) in a frontal orientation. Samples were stained with H&E following to standard protocols. To quantify brain vacuolization, the number of vacuoles with diameters > 5 μm was counted for all sections spanning the entire fly brain.

Apoptotic cell death was assessed by TUNEL staining on cryosections of heads from adult flies using the *in situ* cell death detection kit (Roche). Adult heads were separated from the bodies and fixed in PBS containing 4% formaldehyde for 2 hr at room temperature. After washing with PBS for 1 hr, the fixed heads were cryoprotected in 30% sucrose-PBS solution overnight, embedded into Optimal Cutting Temperature (OCT) compound (Sakura, Japan) and frozen at -80^{o}C. Ten mm thick cryosections were made using a CM3050 S microtome (Leica). The cryosections were washed with PBS and permeabilized in a solution of 0.1% sodium citrate and 0.1% Triton X-100 for 15 min at 4°C. After washing with PBS, cryosections were incubated with TUNEL reaction mixture in the dark for 1 hr at 37°C followed by DAPI staining. For quantification of apoptotic cell death (**Figure 27 and Figure 31**), TUNEL- and DAPI-positive cells were counted in three consecutive, middle frontal sections of the adult brain.

For double-staining of brains with TUNEL and antibodies (**Figure 28, Figure 29 and Figure 31**), whole brains were dissected in PBS and immediately fixed in PBS containing 4% formaldehyde for 1 hr. Fixed brains were with PBS and permeabilized in a solution of 0.1% sodium citrate and 0.1% Triton X-100 for 30 min. After washing with PBS, samples were incubated with TUNEL reaction mixture in the dark for 1 hr at 37°C. The samples were washed with PBT-0.3 (PBS, 0.3% Triton X-100), blocked with PBT-0.3 containing 5% BSA, and then incubated with primary antibodies for 2 days at 4°C. After washing with PBT-0.3 containing 5% BSA for 1 hr at room temperature, samples were incubated with secondary antibodies overnight at 4°C. The following antibodies were used in this study: anti-Elav (9F8A9) at 1:10, anti-Repo (8D12) at 1:10, anti-P-Mad at 1:100, and anti-cleaved caspase-3 (Cell Signaling) at 1:100.

8. Adult Behavioral Analysis

Adult flies aged for 20 days were tested for locomotor ability in an adult climbing assay (Ellis *et al*., 2010). For each genotype, 100 individual flies were collected and placed into an empty glass cylinder with a line drawn 2 cm from the bottom. After acclimate to its environment for 5 min, flies were gently vortexed and the number of flies that climbed above the 2-cm mark after 30 sec was counted. Five separate and consecutive trials were performed, and the results were averaged.

9. Statistical Analysis

Data are presented as mean ± SEM. The numbers of samples analyzed

are indicated inside the bars or in the figure legends. To determine statistical significance, I applied one-way ANOVA followed by post hoc pair-wise comparisons of means using Tukey-Kramer test.

III. Results

1. Generation of *spartin* Null Mutant

A BLASTP search of the *Drosophila* genome identified a single homolog of human Spartin (CG12001). Sequence alignment analysis showed that the predicted *Drosophila* Spartin has an identical domain organization and overall 21% identity and 44% similarity to its human counterpart **(Figures 1A and 1B)**. To investigate the *in vivo* functions of Spartin, the disrupted *spartin* gene by imprecise excision of an EP element (G8635) inserted in the 3' untranslated region of the adjacent *karyβ3* gene **(Figure 2A)**. One imprecise excision, which we refer to as $spartin^{1}$, had a 1,957-bp deletion that begins from the site of EP insertion and extends into the second exon of *spartin*. Homozygous $spartin^{1}$ animals as well as animals transheterozygous for $spartin^{1}$ and the deficiency *Df(3R)110* (hereafter refer to as *Df*) deleting the *spartin* locus were viable and fertile. In these animals, *spartin* but not *karyβ3* RNA expression was abolished **(Figure 2B)**, suggesting that $spartin^{1}$ represents a null allele for the *spartin* gene.

2. Spartin Is Localized Presynaptically at the NMJ

To determine the expression pattern and subcellular distribution of Spartin, I generated a polyclonal antibody against its segment (amino acids 102-202). In western blot analysis of lysates derived from wild-type third instar larvae, the antibody recognized a band of ~67 kDa, corresponding to the expected size for *Drosophila* Spartin **(Figures 3A and 3A)**. The 67 kDa product was not detected in *spartin* mutant larvae extracts and significantly

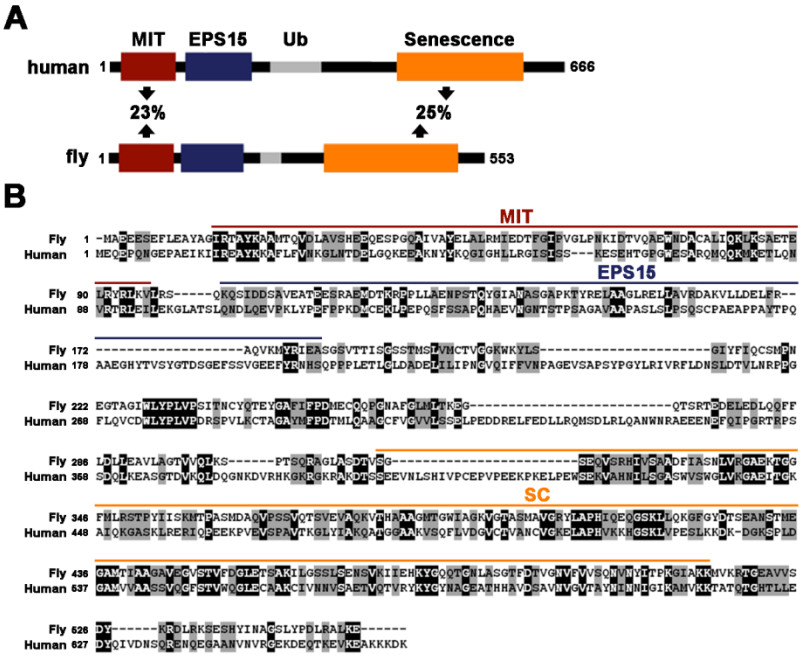
A
MIT
EPS15
Ub
Senescence
human 1
666
23%
25%
fly 1
553
B
MIT
EPS15
SC
Fly 1
Human 1
Fly 90
Human 88
Fly 172
Human 178
Fly 222
Human 268
Fly 286
Human 358
Fly 346
Human 448
Fly 436
Human 537
Fly 526
Human 627

Figure 1. Domain Structures of Human and *Drosophila* Spartin

(A) Domain structures of human Spartin and its *Drosophila* ortholog with the percent identity between their corresponding domains. Abbreviations of Spartin domains are as follows: MIT (red), contained in microtubule-interacting and trafficking proteins; Eps15 (blue), Eps15-interacting domain; Senescence (orange), plant-related senescence domain (http://smart.emblheidelberg.de). (B) Alignment of *Drosophila* and human Spartin proteins shows identical residues indicated by white letters on a black background. Conserved residues are indicated by black letters on a gray background.

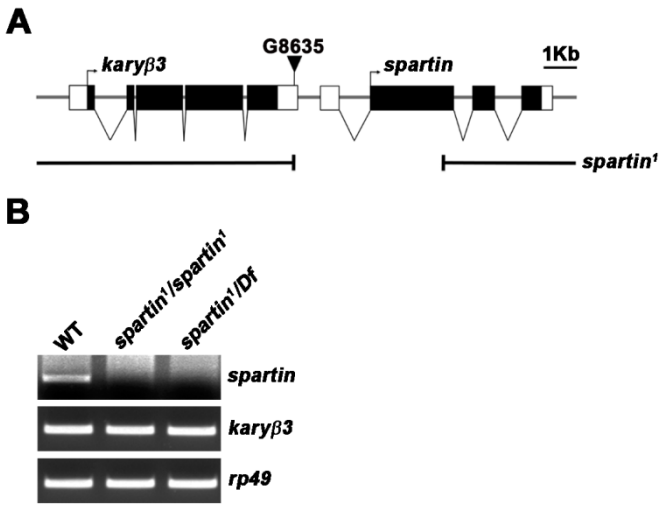

Figure 2. Molecular Characterization of *Drosophila spartin* and Mutants

(A) Genomic organization of the *spartin* locus. The exon/intron organization of *spartin* and its neighboring gene, *karyβ3,* shown along with the position of P-element G8635 (inverted triangle). Introns are indicated by horizontal lines, exons by boxes, and coding regions by black boxes. Translation initiation sites are indicated by arrows. Shown below is the *spartin*^{1} deletion generated by imprecise excision of G8635. (B) RT-PCR analysis of *spartin*, *karyβ3* and *rp49* in third instar wildtype (WT), *spartin*^{1}*/spartin*^{1} and *spartin*^{1}*/Df(3R)110* (*spartin*^{1}*/Df*) larvae.

reduced in S2R+ cells treated with *spartin* dsRNA, indicating the specificity of our anti-Spartin antibody. Using this antibody, I performed immunohistochemistry to examine the expression pattern of Spartin of embryos and third instar larval fillets. In the immunohistochemistry analysis, Spartin was detected broadly in the embryos but localized to the plasma membrane of the embryos at cellular blastoderm stages (stage 5) **(Figure 3B)**. At embryonic stage 13, Spartin was found to be in the brain, the salivary gland and gut **(Figure 3C)**. Spartin was totally absent in *spartin*^{1}*/Df* mutant embryos **(Figure 3D)**. I also analyzed the synaptic protein synaptotagmin I revealed that Spartin was expressed in the synaptic neuropil regions of the larval brain and ventral nerve cord (VNC) **(Figures 3E and 3F)**. Spartin was particularly enriched at the NMJs, but was not detectably expressed in the cytoplasm of body-wall muscles. Double labeling with an antibody against the axonal membrane marker HRP revealed that Spartin is mainly associated with the presynaptic membrane, with a small portion localized to the central region of the boutons **(Figure 4A)**. Spartin was not detected in the NMJ of *spartin*^{1}*/Df* **(Figure 4B)**. At the presynaptic membrane, Spartin was not colocalized with active zone marker Bruchpilot/Nc82, but rather localized in distinctive domains adjacent to active zones **(Figure 4C)**. Spartin was substantially overlapped with the endocytic protein synaptojanin and the early endosome marker Rab5 **(Figures 4D and 4E)**. To further define the subcellular localization of Spartin, I expressed GFP-tagged Rab5 in *Drosophila* S2R+ cells. I observed strong localization between endogenous and GFP-Rab5 on the plasma membrane and in intracellular punctate structures **(Figure 4F)**.

Consistent with previous reports, a small portion of anti-Spartin signals was detected on the surface of lipid droplets in S2R+ cells **(Figure 4F,**

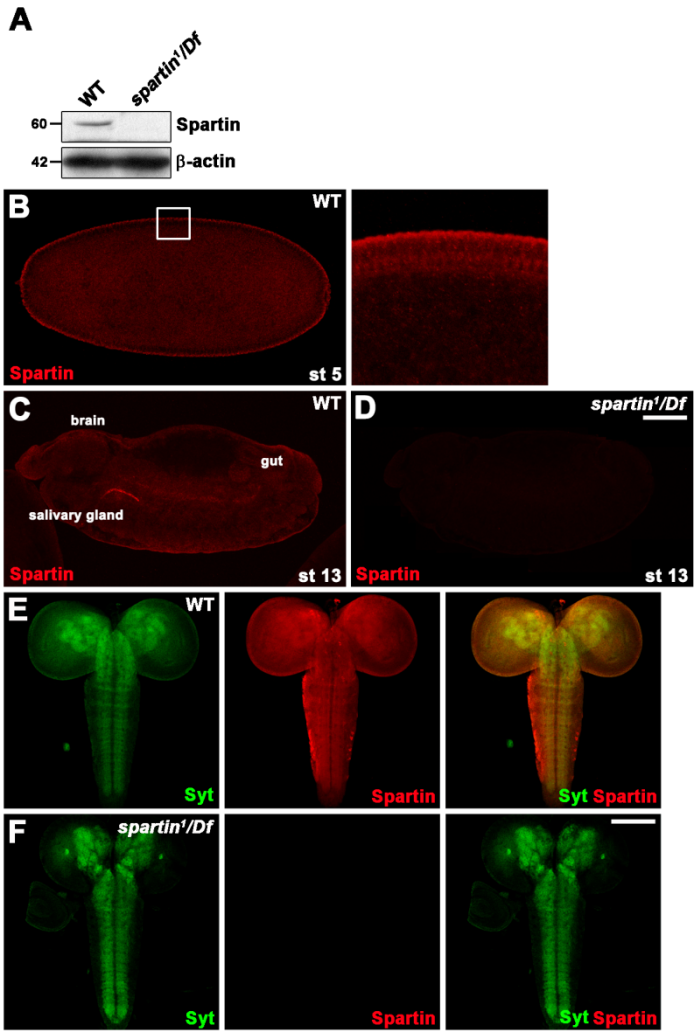
A
WT
spartin¹/Df
60
42
Spartin
β-actin
B
WT
Spartin
st 5
C
WT
brain
gut
salivary gland
Spartin
st 13
D
spartin¹/Df
Spartin
st 13
E
WT
Syt
Spartin
Syt Spartin
F
spartin¹/Df
Syt
Spartin
Syt Spartin

Figure 3. Patterns of Spartin Expression in Embryos and Larval Brains

(A) Western blotting of total extracts prepared from wildtype and *spartin*^{1}*/Df* third instar larvae with anti-Spartin and anti-β-actin. The Spartin antibody detects a single protein of 60 kDa in the extract of wildtype larvae, but not in the extract of *spartin*^{1}*/Df* mutant larvae. (B-C) Whole mount wildtype and *spartin*^{1}*/Df* embryos stained by anti-Spartin. Lateral view of late stage 5 (B) and stage 13 (C) embryos. Spartin protein was ubiquitously expressed at early stages, and distributes in the salivary gland, brain and gut at late stages. (D) Lateral view of a stage 13 *spartin*^{1}*/Df* embryos stained by anti-Spartin. (E) Confocal images of the CNS dissected from third instar wildtype (WT) and *spartin*^{1}*/Df* larvae co-labeled by anti-Spartin (red) and anti-synaptotagmin I (green) antibodies. (F) The *spartin*^{1}*/Df* mutant larvae brain does not show Spartin immunoreactivity at detectable levels. Scale bars, 50 μm (D), 100 μm (F).

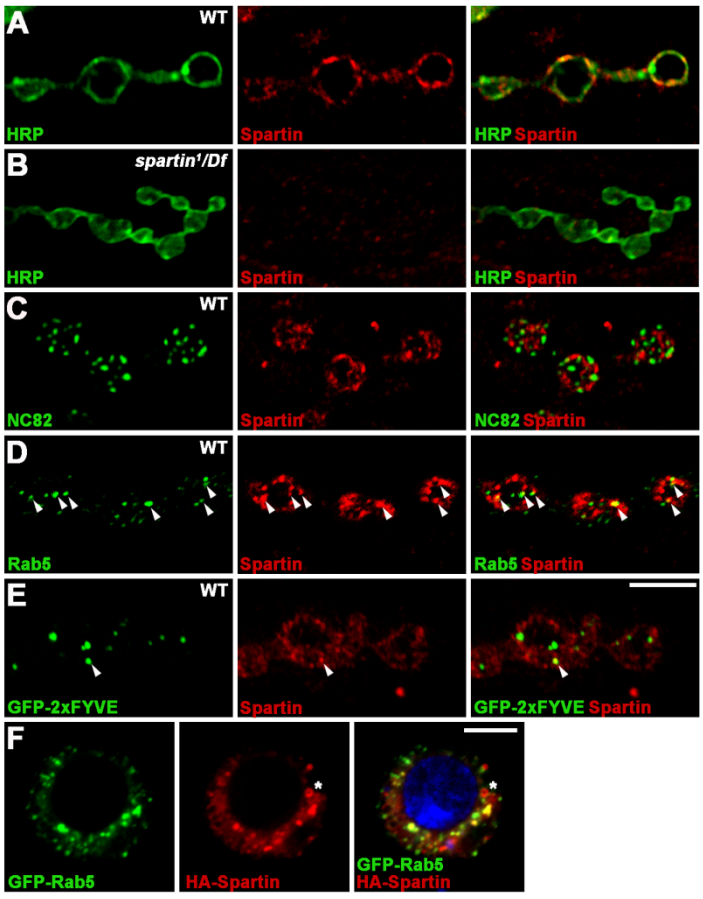
A
WT
HRP
Spartin
HRP Spartin
B
spartin¹/Df
HRP
Spartin
HRP Spartin
C
WT
NC82
Spartin
NC82 Spartin
D
WT
Rab5
Spartin
Rab5 Spartin
E
WT
GFP-2xFYVE
Spartin
GFP-2xFYVE Spartin
F
GFP-Rab5
HA-Spartin
GFP-Rab5
HA-Spartin

Figure 4. Spartin Localizes to the Presynaptic Compartment of *Drosophila* NMJ

(A-B) Single confocal slices of NMJ 6/7 branches with type I boutons doubly stained with anti-Spartin (red) and anti-HRP (green) are shown for wildtype (WT) and *spartin*^{1}*/Df* mutant larvae. Spartin protein is mainly expressed in presynaptic region and Spartin immunoreactivity is almost undetectable in *spartin*^{1}*/Df* larvae. (C) Wildtype double stained with anti-NC82 (green) and anti-Spartin (red) antibodies. At the presynaptic membrane, Spartin was not colocalized with the active zone marker NC82. (D) Confocal images of NMJ 6/7 labeled with anti-HRP (green) and anti-Rab5 (red). (E) Third instar larvae expressing GFP-2xFYVE driven by *C155-GAL4* are doubly stained with anti-Spartin and anti-GFP. Spartin was substantially overlapped with the endocytic protein synaptojanin throughout boutons and partially with the early endosome marker Rab5 in the lumen of bouton. Arrowheads show Spartin puncta costained for Rab5 or GFP-2xFYVE. (**F**) A single confocal slice of S2R+ cells doubly stained with anti-Spartin and anti-Rab5 antibodies. Spartin and Rab5 colocalized at the plasma membrane and in the cytoplasmic structures in a punctate pattern. Spartin, but not Rab5, also encircles lipid droplets (asterisk). Scale bars represent 5 μm (E and F).

asterisk). Thus Spartin localizes to distinctive plasma membrane domains and Rab5-postive early endosomes in both NMJ synapses and nonneuronal cells.

3. Spartin Is Required Presynaptically for Normal Synaptic Growth

Given the presynaptic localization of Spartin at the larval NMJ, I wondered if loss of *spartin* might cause defects in synapse development. To test this possibility, I examined the NMJs of third instar *spartin* mutants with anti-HRP antibody, which visualizes neuronal membranes. Compared with wildtype controls (w^{1118}), homozygous $spartin^{1}$ and $spartin^{1}/Df$ mutants displayed a synaptic overgrowth phenotype **(Figure 5A)**. For quantification of this phenotype, I measured overall bouton number, satellite bouton number, and NMJ length at third instar NMJ 6/7 in abdominal segment 2. Bouton number normalized to muscle area was increased by 39% in *spartin* mutants compared with control larvae. At the same time, satellite bouton number and NMJ length normalized to muscle area were increased by 91% and 41%, respectively. Larvae homozygous for $spartin^{1}$ had essentially identical NMJ phenotypes to $spartin^{1}/Df$ **(Figures 5B and 5D)**. Revertant (precise excision of EP element G8635) animals showed normal NMJ morphology. All of these phenotypes were completely rescued by neuronal expression of a HA-tagged *spartin* transgene (*UAS-HA-spartin*) or Myc-tagged human *spartin* (*UAS-Myc-human spartin*) with the panneuronal driver *C155-GAL4* **(Figures 5B and 5D)**. However, expression of the same transgene using the muscle driver *BG57-GAL4* failed to rescue the NMJ phenotypes of *spartin* **(Figures 5B and 5D)**.

In addition, I examined whether Spartin was required in presynaptic for normal NMJ growth using GAL4-inducible RNAi mutants. The presynaptic reduction of Spartin showed defects in NMJ morphology **(Figure 6)**.

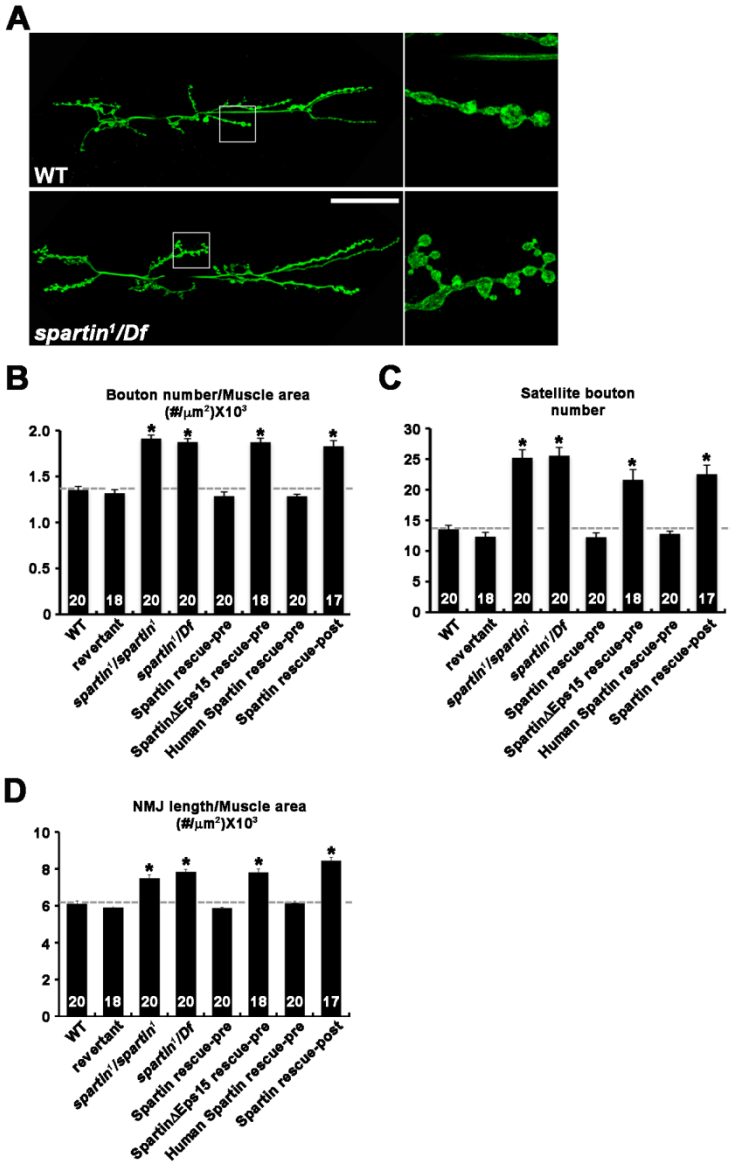
A
WT
spartin¹/Df
B
Bouton number/Muscle area
(#/μm²)X10³
2.0
1.5
1.0
0.5
0
20 18 20 20 20 18 20 17
WT
revertant
spartin¹/spartin¹
spartin¹/Df
Spartin rescue-pre
SpartinΔEps15 rescue-pre
Human Spartin rescue-pre
Spartin rescue-post
C
Satellite bouton
number
30
25
20
15
10
5
0
20 18 20 20 20 18 20 17
WT
revertant
spartin¹/spartin¹
spartin¹/Df
Spartin rescue-pre
SpartinΔEps15 rescue-pre
Human Spartin rescue-pre
Spartin rescue-post
D
NMJ length/Muscle area
(#/μm²)X10³
10
8
6
4
2
0
20 18 20 20 20 18 20 17
WT
revertant
spartin¹/spartin¹
spartin¹/Df
Spartin rescue-pre
SpartinΔEps15 rescue-pre
Human Spartin rescue-pre
Spartin rescue-post

Figure 5. Spartin Functions Presynaptically to Control Synaptic Growth

(A-D) Mutations in *spartin* cause synaptic overgrowth at larval NMJs. (A) Confocal images of NMJ 6/7 at segment A2 are show stained with anti-HRP shown for wildtype (WT) and *spartin*^{1}*/Df* mutant larvae. Scale bar, 50 μm. (B-D) Quantification of overall bouton number normalized to muscle surface area and satellite bouton number in the following genotypes: wildtype, precise excision EP line G8635 (revertant), *spartin*^{1}*/spartin*^{1}, *spartin*^{1}*/Df*, *C155-GAL4/+;Df/UAS-HA-spartin,spartin*^{1} (Spartin rescue-pre), *C155-GAL4/+;Df/UAS-HA-spartinΔEps15,spartin*^{1} (SpartinΔEps15 rescue-pre), *C155-GAL4/+;Df/UAS-Myc-spartin-human,spartin*^{1} (Human Spartin rescue-pre) and *BG57-GAL4,Df/UAS-HA-spartin,spartin*^{1} (Spartin rescue-post). All comparison are with wildtype unless indicated (*$p < 0.001$)

Expression of *spartin*^{RNAi} in *C155-GAL4* induced abnormal synaptic morphology compared to control. The numbers of bouton was 11%, Satellite bouton was 17% increased and all parameters of synaptic overgrowth. After normalization to muscle area, the bouton number is more dramatically increased. But expression of the same *spartin*^{RNAi} in muscles using *BG57-GAL4*, had no effects on synaptic growth. To further characterize the roles of Spartin at NMJ synapses, I analyzed *spartin* gain-of-function mutants. Overexpression of the *UAS-HA-spartin* transgene in the wildtype background, using the *C155-GAL4* driver, significantly reduced overall bouton number and satellite bouton number compared with GAL4 alone ($p < 0.005$ and $p < 0.001$, respectively) **(Figure 8)**. These gain-of-function phenotypes are the opposite of those observed in *spartin* null mutants, revealing an inverse relationship between levels of presynaptic Spartin and extent of synaptic growth. However, postsynaptic overexpression of Spartin had no effect on synaptic transmission. The NMJ morphology of first instar *spartin*^{1}/*Df* larvae at 1 h after hatching was normal **(Figure 7)**, indicating that loss of *spartin* function does not impair initial synapse formation. Thus, Spartin functions in neurons to restrain synaptic growth during postembryonic development.

4. Spartin Is Required Presynaptically for NMJ Neurotransmission

Satellite boutons in *spartin* mutants display the predicted molecular and structural features of a functional synaptic bouton (Nahm *et al*., 2013). I next examined the functional properties of *spartin* null NMJs by measuring postsynaptic currents using two-electrode voltage-clamp (TEVC) recording configuration **(Figures 9A and 9B)**. The evoked excitatory junction currents (EJCs) from third instar NMJs 6/7 was clearly decreased in *spartin* loss-of-

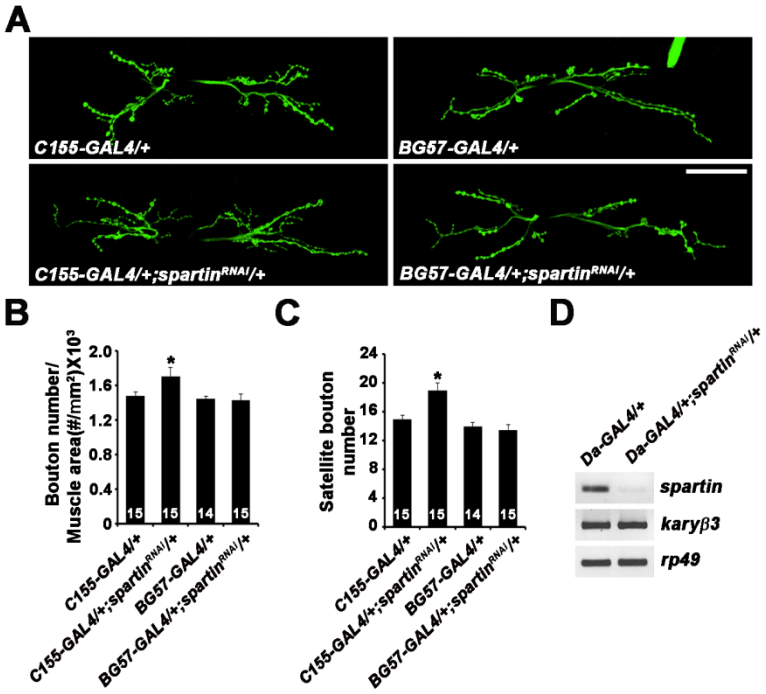
A
C155-GAL4/+
BG57-GAL4/+
C155-GAL4/+;spartinRNAi/+
BG57-GAL4/+;spartinRNAi/+
B
Bouton number/ Muscle area(#/mm²)X10³
2.0
1.6
1.2
0.8
0.4
0
15
15
14
15
C155-GAL4/+
C155-GAL4/+;spartinRNAi/+
BG57-GAL4/+
BG57-GAL4/+;spartinRNAi/+
C
Satellite bouton number
24
20
16
12
8
4
0
15
15
14
15
C155-GAL4/+
C155-GAL4/+;spartinRNAi/+
BG57-GAL4/+
BG57-GAL4/+;spartinRNAi/+
D
Da-GAL4/+
Da-GAL4/+;spartinRNAi/+
spartin
karyβ3
rp49

Figure 6. Presynatic Knockdown of Spartin Causes Overgrowth of the NMJ

(A) Confocal images of NMJs 6/7 labeled with FITC-conjugated anti-HRP. Spartin was knocked-down by expressing *spartin*^{RNAi} in either neuron (*C155-GAL4*) or muscles (*BG57-GAL4*). Scale bar, 50 μm. (B-C). Quantification of bouton number (B), and satellite bouton number (C) at NMJs 6/7 in *C155-GAL4/+*, *C155-GAL4/+; UAS-spartin*^{RNAi}*/+*, *BG57-GAL4/+* and *BG57-GAL4/+; UAS-spartin*^{RNAi}*/+*. The numbers of NMJs analyzed are indicated inside bars. Statistically significant differences versus the control are indicated on top of bars (*$p < 0.001$). (D) Expression of *spartin*, *karyβ3* and *rp49* RNAs was analyzed in *Da-GAL4/+* and *Da-GAL4/+; UAS-spartin*^{RNAi}*/+* larvae by RT-PCR. RT-PCR was performed with total RNA extract of *Da-GAL4/+* and *Da-GAL4/+; UAS-spartin*^{RNAi}*/+* mutants.

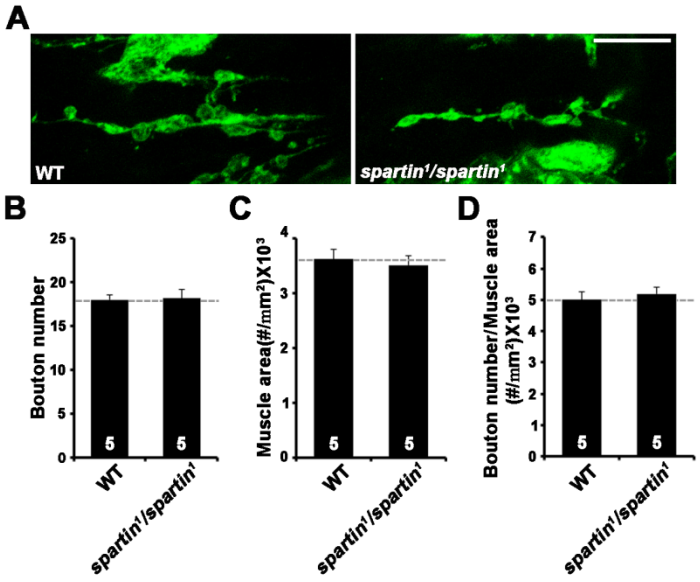

Figure 7. NMJ Growth Is Normal in First Instar *spartin* Larvae

(A) Confocal images of NMJs 6/7 stained with anti-HRP are shown for wildtype and *spartin*^{1}/*spartin*^{1} early first instar larvae (within 1 h after hatching). Scale bar, 10 μm. (B-D) Quantification of total bouton number (B), combined surface area of muscle 6/7 (C), and bouton number normalized to muscle surface area (D). Statistically significant differences versus wildtype are indicated. Error bars indicate mean ± SEM.

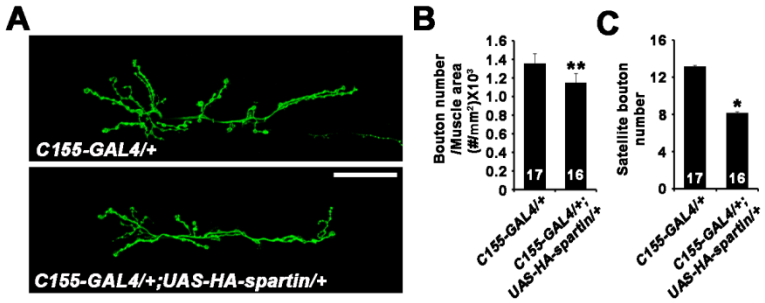

Figure 8. Neuronal Overexpression in *spartin* Induce Synaptic Undergrowth at the NMJ

(A) Confocal images of NMJ 6/7 of larval abdominal segment 2, stained for the HRP shown for *C155-GAL4/+* and *C155-GAL4/+; UAS-HA-spartin/+*. Compared with *C155-GAL4/+*, *C155-GAL5/+; UAS-HA-spartin/+* exhibit a decrease in bouton number and satellite bouton number. Scale bar, 50 μm. (B-C) Quantification of bouton number normalized to muscle surface are (B) and satellite bouton number (C). Significant differences, as determined by Student's *t*-test, are marked on top of bar (*$p < 0.001$; **$p < 0.05$).

function mutants compared with wildtype controls (wildtype: 345 ± 11.1 nA; *spartin*^{1}/*spartin*^{1}: 204 ± 9.3 nA, $p < 0.001$; *spartin*^{1}/*Df*: 230 ± 6.3 nA, $p < 0.001$; **Figure 9A**). To determine whether this defect is caused by a loss of evoked glutamate release from the presynaptic terminal or impaired glutamate receptor function in the postsynaptic compartment, wildtype HA-Spartin was driven independently in either the motor neuron or muscle. Qualitatively, presynaptic rescue was able to strongly rescue the depressed transmission characterizing the *spartin*^{1}/*Df* condition, whereas postsynaptic expression of *spartin* had absolutely no effect **(Figure 9A)**. In quantified comparisons on mean EJC amplitudes, presynaptic rescue restored the response to 290 ± 9.5 nA (p = 0.0001 from *spartin*^{1}/*spartin*^{1}) whereas postsynaptic expression remained at 186 ± 9.7 nA **(Figure 9A)**. These data indicate that *spartin* is required presynaptically but not postsynaptically for evoked glutamatergic synaptic function. Spontaneous mEJCs were also examined to further differentiate pre- versus postsynaptic mechanisms. A change in mEJC amplitude is usually considered due to a change in postsynaptic glutamate receptor numbers or function, whereas a change in mEJC frequency is considered due to a change in the number of presynaptic active zone or probability of synaptic vesicle fusion. Representative 3 s samples of spontaneous mEJCs for each of the five genotypes are shown in **Figure 9B**. Compared with wildtype controls, the amplitudes of spontaneous mEJCs were not significantly changed in *spartin* mutants (wildtype, 0.78 ± 0.03 nA; *spartin*^{1}/*spartin*^{1}, 0.87 ± 0.05 nA; *spartin*^{1}/*Df*, 0.78 ± 0.05 nA), further confirming that it is not working postsynaptically. However, mEJC frequency was clearly decreased in *spartin* mutants (wildtype: 3.4 ± 0.18 Hz; *spartin*^{1}/*spartin*^{1}: 2.2 ± 0.21 Hz, p= 0.0002; *spartin*^{1}/*Df*: 2.78 ± 0.18 Hz, p= 0.02; **Figures 9C and 9D**). This phenotype

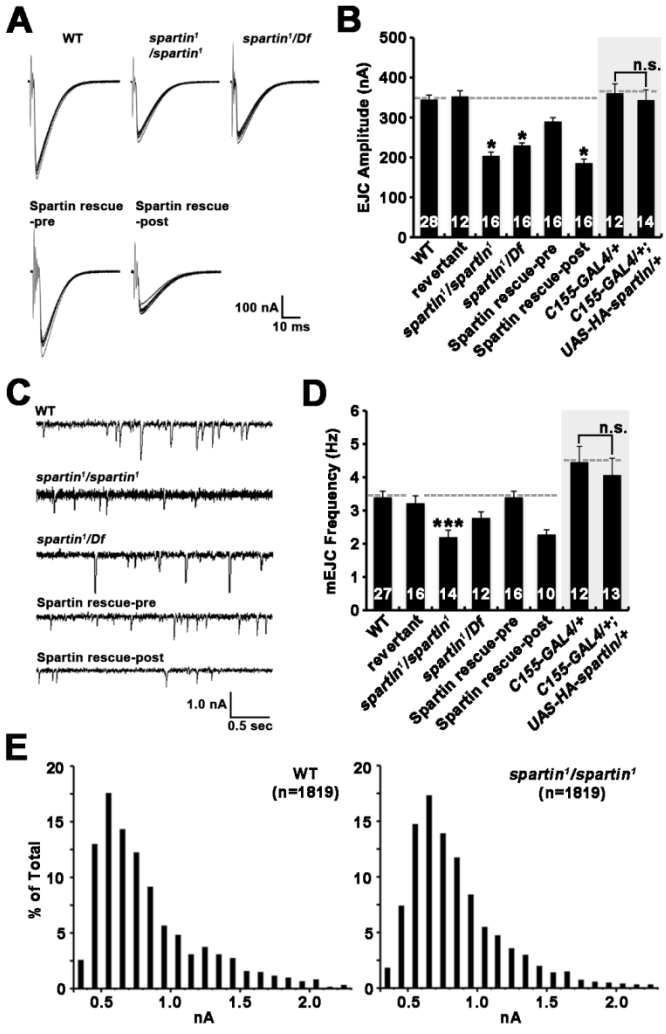
A
WT
spartin¹ /spartin¹
spartin¹/Df
Spartin rescue -pre
Spartin rescue -post
100 nA
10 ms
B
EJC Amplitude (nA)
500
400
300
200
100
0
n.s.
28
12
16
16
16
16
12
14
WT
revertant
spartin¹/spartin¹
spartin¹/Df
Spartin rescue-pre
Spartin rescue-post
C155-GAL4/+
C155-GAL4/+; UAS-HA-spartin/+
C
WT
spartin¹/spartin¹
spartin¹/Df
Spartin rescue-pre
Spartin rescue-post
1.0 nA
0.5 sec
D
mEJC Frequency (Hz)
6
5
4
3
2
1
0
n.s.
***
27
16
14
12
16
10
12
13
WT
revertant
spartin¹/spartin¹
spartin¹/Df
Spartin rescue-pre
Spartin rescue-post
C155-GAL4/+
C155-GAL4/+; UAS-HA-spartin/+
E
WT
(n=1819)
spartin¹/spartin¹
(n=1819)
% of Total
20
15
10
5
0
0.5
1.0
1.5
2.0
nA

Figure 9. Presynaptic Loss of Spartin Impairs NMJ Synaptic Transmission

(A) Representative evoked EJCs from wandering third instar NMJ (1.0 mM Ca^{2+}) for wildtype, *spartin*^{1}*/spartin*^{1}, *spartin*^{1}*/Df*, and presynaptic/postsynaptic expression of wildtype *spartin* in the *spartin*^{1}*/Df* background. Each family of traces shows ten consecutive evoked EJC responses from a 0.2 Hz stimulus train. (B) Quantification of mean evoked EJC amplitude for all five genotypes. Bars indicate mean values with standard error, and significance comparisons as indicated in each case. (C) Representative traces of spontaneous mEJCs. Each record shows a typical 3-second sample from a two minute recording session. (D) Mean frequency of spontaneous mEJCs for all five genotypes. Significance is shown between control and *spartin*^{1} mutants, and between *spartin*^{1} mutant and presynaptic and postsynaptic rescue conditions. P-values marked as (****) for $0.0005 > p > 0.0001$ and as (*) for $0.05 > p > 0.01$, or as not significant (n.s). The sample size was $n \geq 10$ animals for each genotype. Error bars indicate mean +/- s.e.m. (E) Distributions of spontaneous mEJC amplitudes in wildtype and *spartin*^{1}*/spartin*^{1} third instar larvae. Each single event peak from five pooled recordings was binned at 0.1 nAmps to form the frequency of event amplitude.

This figure was provided as part of collaboration with Dr. Kendal Broadie and William Parkinson (Vanderbilt University).

was rescued with presynaptic expression of *spartin*, but not with postsynaptic expression, in the *spartin*^{1}/*Df* background. The presynaptic rescue restored mEJC frequency to 3.4 ± 0.18 Hz (p = 0.0001 from *spartin*^{1}/*spartin*^{1}), whereas postsynaptic expression still resulted in 2.28 ± 0.14 Hz **(Figure 9C)**. The distribution of mEJC amplitudes was indistinguishable between control and *spartin* mutants (Kolmogorov-Smirnov test, p = 0.95) **(Figure 9E)**. These data indicate that *spartin* is required presynaptically but not postsynaptically to maintain the normal frequency of synaptic vesicle fusion events driving glutamatergic synaptic function.

5. Spartin Interacts with Eps15 to Regulate Synaptic Growth and Synaptic Endocytosis

Human Spartin interacts with the endocytic and trafficking protein Eps15 *in vitro* (Bakowska *et al*., 2005). As an initial step to understand the cellular mechanism underlying Spartin function at NMJ synapses, I verified interactions between *Drosophila* Spartin and Eps15. At the *Drosophila* NMJ, *eps15*-null mutants exhibit a synaptic overgrowth phenotype similar to that of *spartin* mutants (Koh *et al*., 2007). This phenotypic similarity, combined with the proved Spartin-Eps15 interaction, strongly suggests a functional relationship between two proteins at the NMJ. To test this possibility, I examined transheterozygous interaction between *spartin* and *eps15*. Heterozygotes that lack one copy of *spartin* and *eps15* alone did not show apparent defects in NMJ growth. However, overall bouton number and satellite bouton formation were significantly increased in *spartin-eps15* transheterozygotes compared with wild-type controls **(Figure 10)**. In addition, Spartin interacts physically with Eps15 (Nahm *et al.*, 2013), suggesting that

they function in the same pathway. *Drosophila* Eps15 plays an essential role in synaptic vesicle endocytosis at the NMJ (Koh *et al*., 2007). To test whether Spartin would be also involved in the same process, I performed FM1-43FX styryl dye uptake experiments in which NMJ synapses were stimulated by 90 mM K^+ **(Figure 11).** During a 1 min labeling period, dye uptake was decreased by ~50% in *spartin^1/Df* mutant animals compared with wildtype. When challenged with the dye in the presence of 5 mM K^+ to determine background dye uptake, both wildtype and *spartin* mutant NMJs showed very low levels of dye uptake compared with mutant NMJs stimulated with 90 mM K^+. The defect in FM1-43FX uptake in the *spartin* mutant was fully rescued by presynaptic expression of wildtype HA-Spartin. Transheterozygous interaction between *spartin* and *eps15* was also observed during the process of FM1-43FX uptake, further supporting that they function in the same pathway.

To further substantiate a functional relationship between Spartin and Eps15, I asked whether the Eps15-binding domain in Spartin is required for its function *in vivo*. To do so, I assessed whether neuronal overexpression of HA-SpartinΔEps15 would rescue the synaptic phenotypes of *spartin* mutants. I found that defects in synaptic growth and synaptic vesicle endocytosis were not restored to normal ranges **(Figure 5 and Figure 11)**. Thus, the Spartin-Eps15 interaction is essential for the role of Spartin in regulating synaptic growth and synaptic endocytosis.

Drosophila Eps15 plays a critical role in maintaining endocytic proteins at NMJ synapse (Koh *et al*., 2007). Based this finding, I next tested whether Eps15 is required for the synaptic targeting of Spartin. I compared distribution of HA-Spartin and HA-SpartinΔEps15 in the *spartin^1/Df* mutant background. Like endogenous Spartin, wild-type HA-Spartin was efficiently

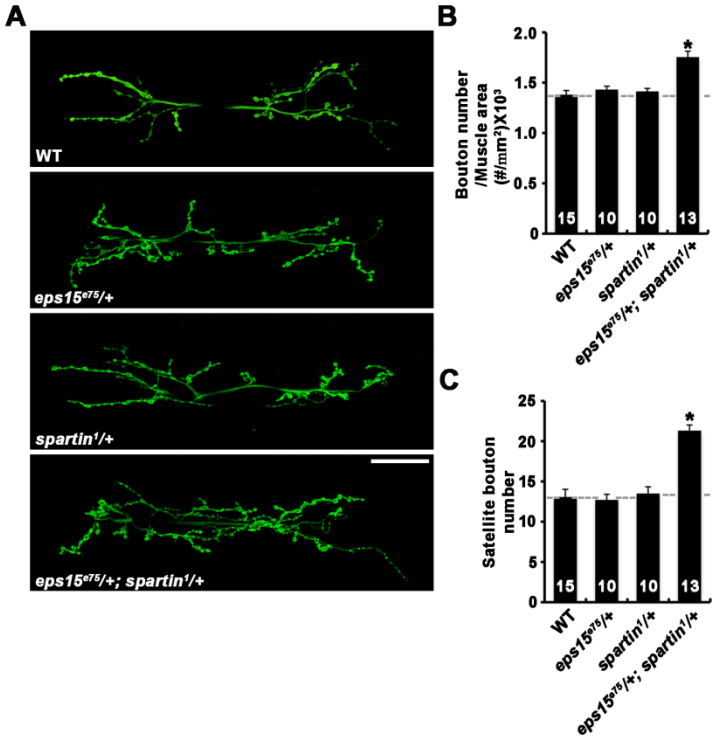

Figure 10. Spartin Interacts with Eps15 to Control Synaptic Growth

(A) Confocal images of NMJs 6/7 labeled with anti-HRP in wildtype (WT), *eps15*^{e75}/+, *spartin*^{1}/+ and *eps15*^{e75}/+; *spartin*^{1}/+ third instar larvae. Compared to wildtype, *eps15*^{e75}/+ and *spartin*^{1}/+ larvae exhibit a significant increase in NMJ length. Scale bar, 50 μm. (B-C) Total bouton number and satellite bouton number were quantified at NMJ 6/7 for wildtype (WT), *eps15*^{e75}/+, *spartin*^{1}/+, and *eps15*^{e75}/+; *spartin*^{1}/+ backgrounds (*$p < 0.001$).

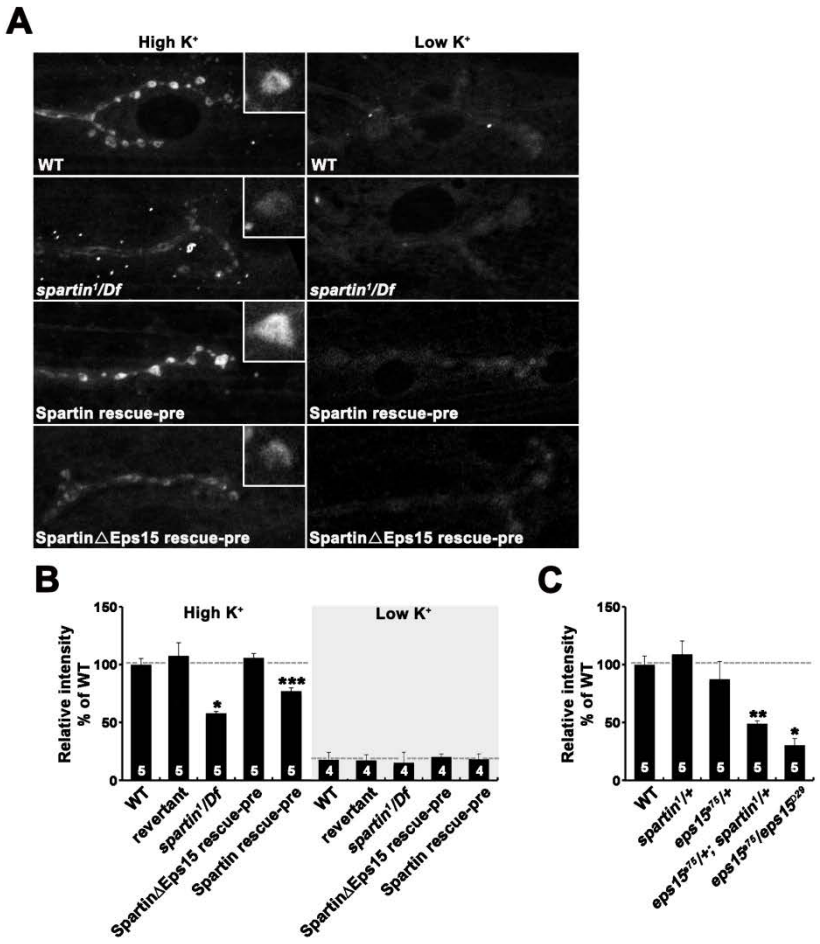
A
High K+
Low K+
WT
WT
spartin1/Df
spartin1/Df
Spartin rescue-pre
Spartin rescue-pre
SpartinΔEps15 rescue-pre
SpartinΔEps15 rescue-pre
B
High K+
Low K+
Relative intensity % of WT
150
100
50
0
5
4
*
***
WT
revertant
spartin1/Df
SpartinΔEps15 rescue-pre
Spartin rescue-pre
C
Relative intensity % of WT
**
*
spartin1/+
eps15P76/+
eps15P76/+; spartin1/+
eps15P76/eps15P29

Figure 11. Spartin Functions with Eps15 to Control Synaptic Vesicle Endocytosis

(A-B) Mutations in *spartin* mutant NMJs show impaired FM1-43FX dye uptake. (A) Representative confocal images of NMJ synapses stimulated with 90 mM K^+ and 5 mM Ca^{2+} in the presence of FM1-43FX. The following genotypes analyzed include wildtype (WT), *spartin*^{1}*/Df, C155-GAL4/+*; *Df/UAS-HA-spartin, spartin*^{1} (Spartin rescue-pre) and *C155-GAL4/+*; *Df/UAS-spartinΔEps15, spartin*^{1} (SpartinΔEps15 rescue-pre). Scale bars, 5 μm. (B) The mean intensities of FM1-43FX labeling in the indicated genotypes are presented as percentages of wildtype larvae. Dye loading was performed in either high-K^+ medium or Ca^{2+}-free, low-K^+ (5 mM) medium. (C) Genetic interaction between *spartin* and *eps15*. FM1-43FX dye were quantified at NMJ 6/7 for wildtype (WT), *spartin*^{1}/+, *eps15*^{e75}/+, *eps15*^{e75}/+; *spartin*^{1}/+ backgrounds and *eps15*^{e75} mutants. The number of larvae examined for each genotype is indicated inside the bars. **p* < 0.001; ***p* < 0.01; ****p* < 0.005.

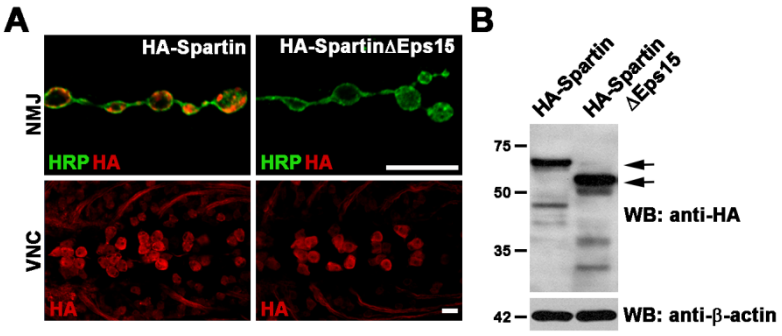

Figure 12. Eps15 Is Required for Efficient Synaptic Localization of Spartin

(A) Single confocal slices of NMJ 6/7 branches and larval ventral nerve cords. Third instar larvae expressing HA-Spartin or HA-SpartinΔEPS15 with *C155-GAL4* in the *spartin*^{1}*/Df* mutant background are doubly stained with anti-HA and anti-HRP. Scale bars, 5 μm. (B) Western blot analysis of larval brain extracts from *C155-GAL4/+; Df/UAS-HA-Spartin, spartin*^{1} and *C155-GAL4/+; Df/UAS-HA-SpartinΔEps15, spartin*^{1}. Anti-β-actin antibody was used as a loading control.

targeted to the NMJ synapse **(Figures 12A and 12B)**. However, HA-SpartinΔEps15 signals were not enriched at the synapse but were largely detected in the soma and within motor axons **(Figure12A)**. In addition, Eps15 is also required for the synaptic localization of Spartin (Nahm *et al*., 2013), confirming that Eps15 recruits Spartin to the NMJ presynaptic terminal through the Spartin-Eps15 interaction.

6. Spartin Inhibits BMP Signaling by Endocytic Downregulation of the Type II BMP Receptor Wit

Recapitulating the *spartin* loss-of-function phenotype is similar to that of elevated BMP signaling induced synaptic overgrowth with excessive satellite bouton formation (O'Connor-Giles et al., 2008; Sweeney and Davia, 2002). I therefore wondered if synaptic overgrowth in *spartin* mutants might be sensitive to BMP signaling. To test this, I examined genetic interactions between *spartin* and components of the BMP pathway. I found that removing one copy of *wit*, which did not alter NMJ morphology by itself, completely reversed the synaptic overgrowth phenotype of *spartin* **(Figure 13)**. In addition, the synaptic overgrowth phenotype of *spartin* was further suppressed by removing both copies of *wit*. Furthermore, the extent of synaptic growth was not significant different between *spartin wit* double mutants and *wit* single mutants **(Figures 13A and 13B)**. Finally, neuronal overexpression of *dad* in the $spartin^{1}/Df$ background also caused a synaptic undergrowth phenotype **(Figure 13C)**. These data indicate that synaptic overgrowth in *spartin* mutants requires normal BMP signaling and further suggest that Spartin restrains synaptic growth by inhibiting presynaptic BMP signaling. To directly confirm the inhibitory effect of Spartin on BMP signaling, I examined accumulation of

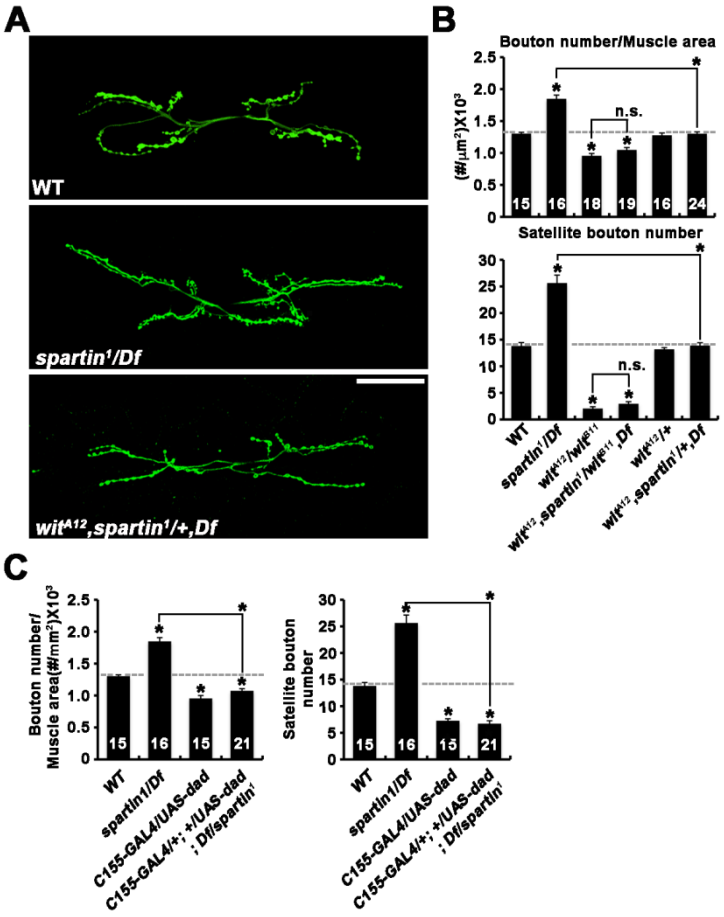
A
WT
spartin¹/Df
wit^A12,spartin¹/+,Df
B
Bouton number/Muscle area
(#/μm²)X10³
n.s.
15
16
18
19
16
24
Satellite bouton number
n.s.
WT
spartin¹/Df
wit^A12/wit^B11
wit^A12,spartin¹/wit^B11,Df
wit^A12/+
wit^A12,spartin¹/+,Df
C
Bouton number/
Muscle area(#/mm²)X10³
Satellite bouton
number
15
16
15
21
WT
spartin1/Df
C155-GAL4/UAS-dad
C155-GAL4/+; +/UAS-dad
; Df/spartin¹

Figure 13. Synaptic Overgrowth in *spartin* Nulls Depends on Levels of BMP Signaling.

(A-C) Genetic upregulation of BMP signaling leads to synaptic overgrowth at larval NMJs. (A) Confocal images of NMJ 6/7 labeled with anti-HRP shown for wildtype (WT), *spartin*^{1}*/Df*; and *wit*^{A12}, *spartin*^{1}/+,*Df* larvae. Scale bar, 50 μm. (B) Quantification of total bouton number normalized to muscle surface area and satellite bouton number at NMJ 6/7 were quantified in the indicated genotypes. (**C**) Quantification of overall bouton number and satellite bouton formation at NMJ 6/7 in the indicated genotypes (wildtype (WT), *spartin*^{1}*/Df*, *C155-GAL4/+; UAS-dad/+* and *C155-GAL4/+; UAS-dad/+; spartin*^{1}*/Df* larvae). Values are normalized to muscle surface area. **p* < 0.001; n.s., not significant (compared with wildtype).

phosphorylated Mad (P-Mad), a well-established readout of BMP signaling levels (O'Connor-Giles *et al*., 2008; Wang *et al*., 2007), in *spartin* mutants. In wildtype larvae, P-Mad immunoreactivity was detected at the terminal and in the nuclei of motor neurons. The average intensities of P-Mad signal at both locations were significantly increased in *spartin* mutants compared with wild type **(Figure 14)**, suggesting that Spartin acts as an inhibitor of BMP signaling in motor neurons.

I then went on to investigate the mechanism by which Spartin inhibits the activity of BMP signaling. Having established the role for Spartin in synaptic vesicle endocytosis, I wondered if Spartin might be also required for the internalization of BMP receptors. To test this possibility, I transiently expressed the Wit-mCherry fusion protein in S2R+ cells, and Wit protein was monitored of cells. I observed robust Wit-mCherry protein and total Wit protein expression at the cell surface and in discrete intracellular puncta **(Figure 15)**. I next assessed the effects of Spartin knockdown on the distribution of Wit. The ratio of surface Wit-mCherry fusion protein and total Wit protein were strongly increased in cell treated with *spartin* dsRNA compared with controls **(Figure 15)**, suggesting that Spartin stimulates the internalization of Wit to limit BMP signaling. In addition, Spartin promotes endosomal trafficking of Wit lysosomes for degradation, and Spartin was involved in the regulation of Wit at the NMJ (Nahm *et al*., 2013). These data suggest that Spartin required for endocytic degradation of Wit, and Spartin functions presynaptically to downregulate Wit at the NMJ.

7. Spartin Regulates Synaptic Growth by Modulating Microtubule Stability through Futsch

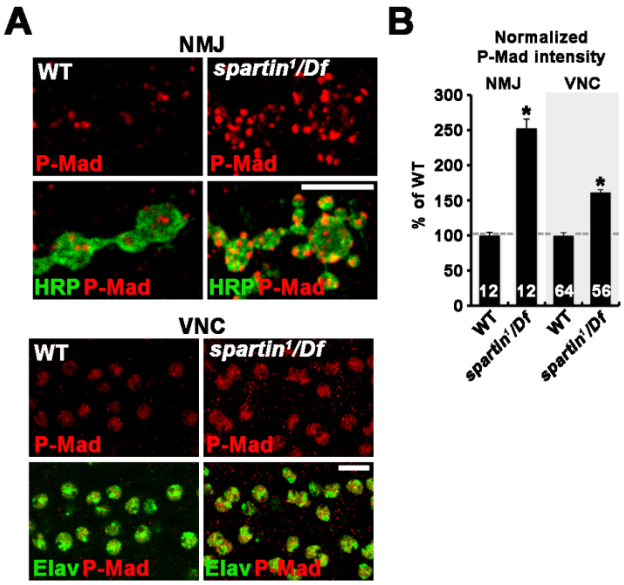

Figure 14. Spartin Is Required for the Proper Accumulation of P-Mad in Motor Neurons

(A) Confocal images of NMJ 6/7 labeled with anti-P-Mad are shown for wildtype and *spartin*^{1}*/Df* larvae. Scale bars 10 μm. (B) Quantification of the ratio of mean P-Mad to HRP levels at the NMJ and in the ventral nerve cord (VNC). Values are percentages of the wildtype. All comparisons are with wildtype unless indicated (*$p < 0.001$). Error bars are SEM for all figures.

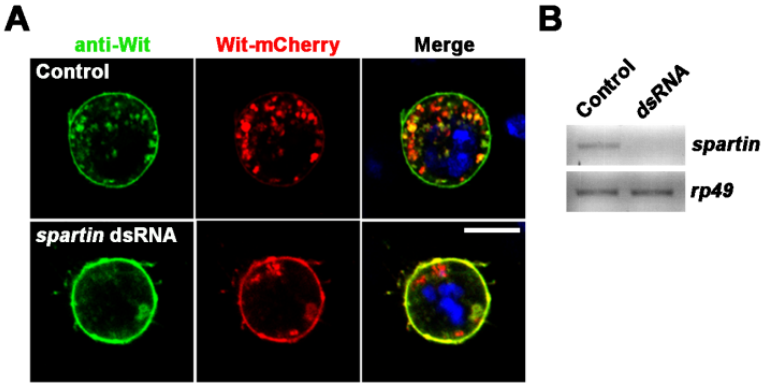

Figure 15. Spartin Required for Endocytic degradation of BMP Receptors

(A) Localization of total Wit protein and Wit-mCherry fusion protein in control or *spartin* dsRNA treated S2R+ cells. Levels of surface Wit-mCherry and total Wit protein are increased by *spartin* depletion. Scale bars 50 μm. (B) RT-PCR was performed with total RNA extract of control and *spartin* dsRNA cell lysates.

At the *Drosophila* NMJ, disruption of BMP signaling decreases the levels of stable microtubules and Futsch (Ellis *et al*., 2010; Wang *et al*., 2007), the *Drosophila* MAP1B homolog that is known to regulate microtubule stability (Bettencourt *et al*., 2005; Roos *et al*., 2000). Given the role for Spartin in inhibiting BMP signaling, I investigated whether loss of Spartin affects microtubule stability and Futsch levels. For this, I first stained third instar larvae with antibodies against acetylated and tyrosinated tubulin markers to visualize stable and unstable microtubules, respectively (Goold *et al*., 1999; Vadlamudi *et al*., 2005; Webster *et al*., 1989). The average intensity of acetylated α-tubulin was increased by 66% in *spartin*^{1}*/Df* compared with wildtype motor axons, while tyrosinated α-tubulin signal was remained unchanged in the mutant **(Figures 16A and 16B)**. I then examined the levels and distribution of axonal and presynaptic Futsch. At wildtype NMJs, anti-Futsch signals were observed as a filamentous structure that runs the center of each synaptic branch **(Figures 16C and 16D)**. Within a subset of boutons, Futsch staining also highlighted loop-like structures **(Figure 16C,** arrows**)**. In *spartin* mutant axons, a Futsch level was increased by 85% compared with wildtype controls ($p < 0.001$; **Figures 16B and 16D**). I also found that the number of futsch-labeled loops per NMJ was significantly increased in *spartin* mutants (wildtype: 20.7 ± 0.8, $n = 10$; *spartin*^{1}*/Df*: 32.2 ± 2.3, $n = 10$, $p < 0.001$). The increase of acetylated α-tubulin and Futsch in motor axons induced by *spartin* mutations was rescued by neuronal expression of either HA-Spartin or HA-human Spartin **(Figures 16B and 16D)**. Similarly in S2R+ cell, I found that acetylated α-tubulin is increased by *spartin* dsRNA **(Figure 17)**. Moreover, Futsch accumulation in *spartin* mutants was strongly suppressed by heterozygosity and hemizygosity for *wit* **(Figure 16D)**, supporting a model in

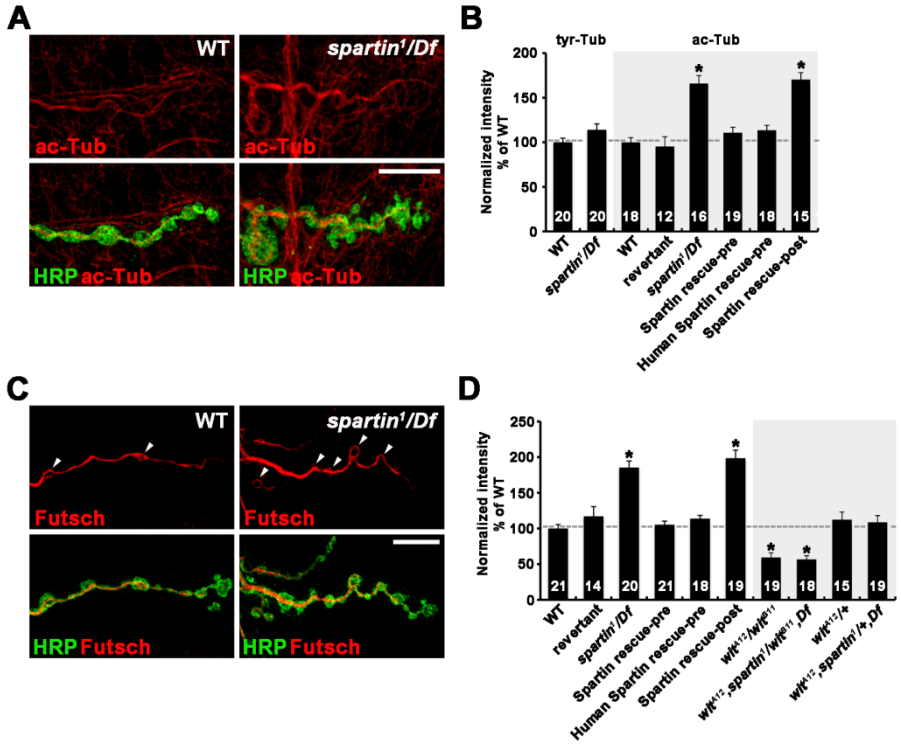
A
WT
spartin¹/Df
ac-Tub
ac-Tub
HRP ac-Tub
HRP ac-Tub
B
tyr-Tub
ac-Tub
Normalized intensity
% of WT
200
150
100
50
0
20
20
18
12
16
19
18
15
WT
spartin¹/Df
WT
revertant
spartin¹/Df
Spartin rescue-pre
Human Spartin rescue-pre
Spartin rescue-post
C
WT
spartin¹/Df
Futsch
Futsch
HRP Futsch
HRP Futsch
D
Normalized intensity
% of WT
250
200
150
100
50
0
21
14
20
21
18
19
19
18
15
19
WT
revertant
spartin¹/Df
Spartin rescue-pre
Human Spartin rescue-pre
Spartin rescue-post
wtᵉ¹¹²/wtᵉ¹¹
wtᵉ¹¹²,spartin¹/wtᵉ¹¹,Df
wtᵉ¹¹²/+
wtᵉ¹¹², spartin¹/+,Df

Figure 16. Spartin Regulates Microtubule Stability in Motor Axons and NMJ Terminals

(A-D) Acetylated α-tubulin and Futsch immunoreactivities are increased in *spartin* mutant axons. (A) Single confocal slices of NMJ 6/7 doubly stained with anti-acetylated α-tubulin and anti-HRP antibodies. (B) Quantification of the average α-tubulin or tyrosinated α-tubulin or acetylated α-tubulin to HRP staining intensities in the following genotypes: wildtype (WT), *spartin*^{1}*/Df*, *C155-GAL4/+;Df/UAS-HA-spartin,spartin*^{1} (Spartin rescue-pre), *C155-GAL4/+;Df/UAS-Myc-spartin-human,spartin*^{1} (Human Spartin rescue-pre), and *BG57-GAL4,Df/UAS-HA-spartin,spartin*^{1} (Spartin rescue-post). (C) Single confocal slices of NMJ 6/7 doubly labeled with anti-Futsch and anti-HRP. The Futsch-labeled loops are indicated by arrowhead. (D) Quantification of the average Futsch to HRP staining intensities in the same genotypes as (B) (*$p < 0.001$). Scale bars, 10 μm.

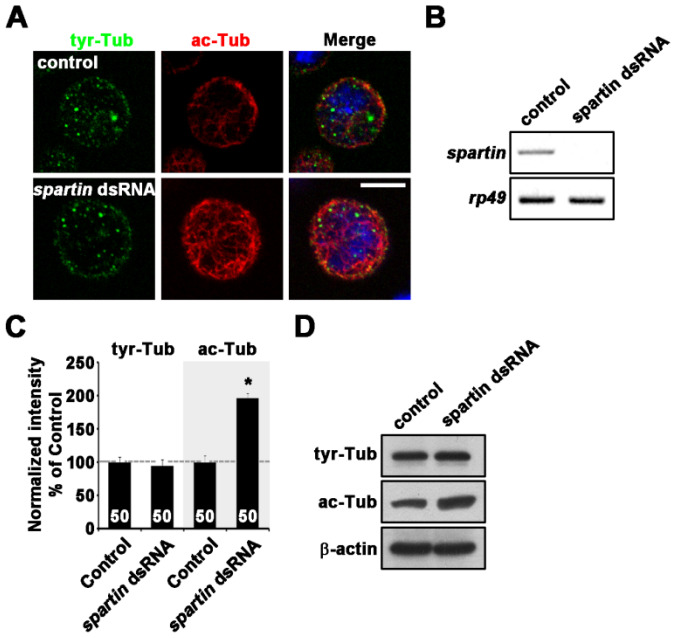

Figure 17. Spartin Decreases Microtubule Stability in Cultured Cells

(A) S2R+ cells, which are mock-treated or treated with *spartin* dsRNA, were stained for tyrosinated and acetylated α-tubulin. Acetlyated α-tubulin immunoreactivities are increased in *spartin* dsRNA treated S2R+ cells. Scale bares, 10 μm (B) The efficiency of *spartin* knockdown was assessed by RT-PCR analysis. (C) Quantification of tyrosinated or acetylated α-tubulin levels in cells. Values are presented as percentages of tyrosinated a-tubulin (*$p < 0.001$). (D) Western blot analysis of total extracts prepared form wildtype and *spartin* dsRNA using antibodies against tyrosinated and acetylated α-tubulin.

which Spartin inhibits BMP signaling to limit presynaptic Futsch levels and microtubule stability. Previous studies have shown that impairments in axonal transport cause the formation of axonal aggregates composed of synaptic components, including mitochondria and vesicles (Hurd and Saxton, 1996). However, despite the defect in microtubule stability, *spartin*-mutant motor neurons do not have general defects in axonal transport (Nahm *et al*., 2013). Futsch-dependent regulation of microtubules is required for normal synaptic growth at the NMJ. For example, animals homozygous for the hypomorphic *futsch*^{k68} allele exhibit synaptic undergrowth at the NMJ (Roos *et al*., 2000).Therefore, I hypothesize that Futsch is a downstream effector of Spartin/BMP signaling in regulating synaptic growth. To test this hypothesis, I first examined genetic interactions between *futsch* and *spartin*. Heterozygosity for *futsch*^{k68} exhibited no or mild effect on overall bouton number and satellite bouton formation in a wildtype background. However, the same heterozygosity significantly suppressed synaptic overgrowth in *spartin*^{1}*/Df* mutants **(Figure 18)**. Furthermore, the *spartin* phenotype was further suppressed by homozygous mutation for *futsch*^{k68}, recapitulating the *futsch*^{k68} phenotype **(Figures 18A and 18C)**. These results suggest that Spartin restrains synaptic growth by inhibiting Futsch. I also examined genetic interactions between *futsch* and mutations in BMP pathway components. Synaptic growth was normal or slightly decreased in heterozygotes for *gbb*, *wit*, and *mad*. In contrast, bouton number and satellite bouton formation were significantly decreased by transheterozygous combinations between *futsch* ^{k68} and *gbb*^{1}, *wit*^{A12}, or *mad*^{273}, suggesting that Futsch acts in the BMP pathway to regulate synaptic growth **(Figures 18D and 18E)**. Combined with previous reports that synaptic Futsch levels are positively regulated by BMP signaling, our data suggest that Futsch acts as a downstream

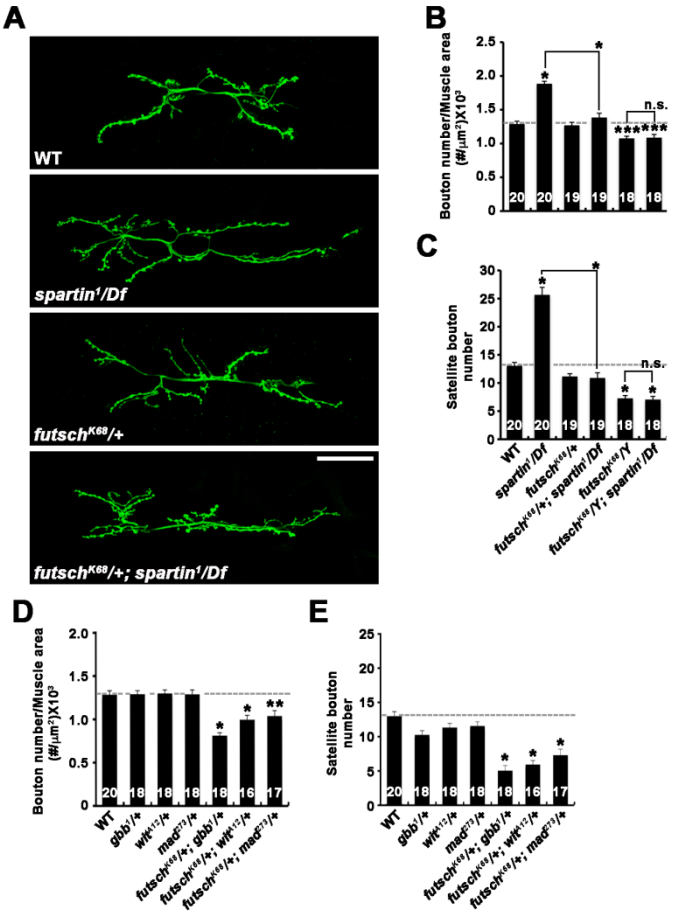
A
WT
spartin¹/Df
futschK68/+
futschK68/+; spartin¹/Df
B
Bouton number/Muscle area (#/μm²)X10³
n.s.
20 20 19 19 18 18
C
Satellite bouton number
n.s.
20 20 19 19 18 18
WT
spartin¹/Df
futschK68/+
futschK68/+; spartin¹/Df
futschK68/Y
futschK68/Y; spartin¹/Df
D
Bouton number/Muscle area (#/μm²)X10³
20 18 18 18 18 16 17
WT
gbb¹/+
wit¹¹²/+
mad²⁷³/+
futschK68/+; gbb¹/+
futschK68/+; wit¹¹²/+
futschK68/+; mad²⁷³/+
E
Satellite bouton number
20 18 18 18 18 16 17
WT
gbb¹/+
wit¹¹²/+
mad²⁷³/+
futschK68/+; gbb¹/+
futschK68/+; wit¹¹²/+
futschK68/+; mad²⁷³/+

Figure 18. Genetic Interactions Between *spartin*, *futsch*, and Mutations of BMP Pathway Components

(A) Confocal images of NMJ 6/7 labeled with anti-HRP are shown for wildtype (WT), *spartin^{1}/Df, futsch^{K89}/+, futsch^{K68}/+; spartin^{1}/Df, Futsch^{K68}/Y and futsch^{K68}/Y; spartin^{1}/Df* larvae. Scale bars 50 μm. (B-C) Quantification of synaptic structural growth at NMJ 6/7 in indicated genotypes. (D-E) Quantification of total bouton number (D), satellite bouton number (E) at NMJs 6/7 in the following genotypes: wildtype (WT), *gbb^{1}*/+, *wit^{A12}*/+, *mad^{273}*/+, *futsch^{K68}*/+*; gbb^{1}*/+, *futsch^{K68}*/+*; wit^{A12}*/+ and *futsch^{K68}*/+*; mad^{273}*/+. Numbers of NMJs analyzed are indicated inside bars. Statistically significant differences versus the wildtype control are indicated on top of bars (*$p < 0.001$; **$p < 0.01$; ***$p < 0.05$; n.s., not significant).

effector of BMP signaling during synaptic growth. To directly assess the involvement of microtubule stability in the Spartin/BMP dependent regulation of synaptic growth, I used the microtubule-severing drug vinblastine (VB). When fed with vinblastine at a concentration that does not affect synaptic growth in wildtype animals, *spartin* mutant larvae display normal synaptic growth **(Figures 19A and 19C)**. Similarly, the synaptic overgrowth phenotype caused by presynaptic expression of constitutively active Tkv (Tkv^{CA}) or *dad* mutations was also completely or significantly rescued by vinblastine treatment **(Figures 19B and 19C)**. In addition, I found that vinblastine suppressed the accumulation of acetylated α-tubulin and Futsch in $spartin^{1}/Df$ mutants in dosage dependent manner **(Figure 20)**. Collectively, our data are consistent with the model in which Spartin and BMP signaling regulate synaptic growth largely by modulating microtubule stability via their effects on presynaptic Futsch.

8. Spartin and BMP Signaling Regulate the Expression of dFMR1, a Negative Regulator of Futsch

How do Spartin and BMP signaling regulate presynaptic Futsch? The *Drosophila* homolog of fragile X mental retardation 1 (dFMR1) has been shown to regulate synaptic growth by repressing the expression of Futsch (Zhang *et al*., 2001). Consistently, loss-of-function mutations in *dfmr1* induces an increase in overall bouton number and satellite bouton number (Nahm *et al*., 2013; Zhang *et al*., 2001), recapitulating the *spartin*-null phenotype. Therefore, I wondered whether the roles for Spartin and BMP in synaptic growth regulation might be linked to dFMR1. To test this possibility, I first examined transheterozygous interactions between *dfmr1* and *spartin* or *dad*. In

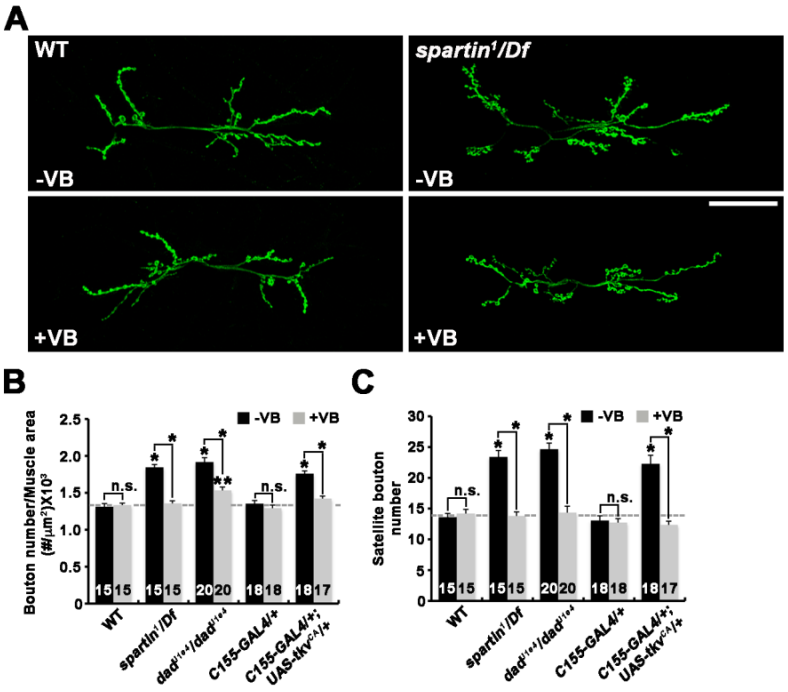
A
WT
-VB
spartin¹/Df
-VB
+VB
+VB
B
Bouton number/Muscle area (#/μm²)X10³
-VB
+VB
n.s.
n.s.
15 15 15 15 20 20 18 18 18 17
WT
spartin¹/Df
dad¹ʳᵉ⁴/dad¹ʳᵉ⁴
C155-GAL4/+
C155-GAL4/+; UAS-tkvᶜᴬ/+
C
Satellite bouton number
-VB
+VB
n.s.
n.s.
15 15 15 15 20 20 18 18 18 17
WT
spartin¹/Df
dad¹ʳᵉ⁴/dad¹ʳᵉ⁴
C155-GAL4/+
C155-GAL4/+; UAS-tkvᶜᴬ/+

Figure 19. Vinblastine Administration Suppresses Synaptic Overgrowth Caused by *spartin* Mutations or Overactivation of BMP Signaling

(A) Confocal images of NMJ 6/7 stained with anti-HRP are shown for wildtype and *spartin*^{1}*/Df* larvae grown in the absence (-VB) or presence (+VB) of vinblastine. (B-C) Quantification of normalized bouton number and satellite bouton at NMJ 6/7 in the indicated genotypes grown in the absence or presence of vinblastine. Genotypes include wildtype (WT), *spartin*^{1}*/Df*, *dad*^{J1e4}*/dad*^{J1e4}, *C155-GAL4/+* and *C155-GAL4/+; UAS-tkv*^{CA}*/+*. All comparisons are with wildtype unless indicated all comparisons are with wildtype unless indicated (*$p < 0.001$; **$p < 0.01$; n.s., not significant). Scale bars, 10 μm.

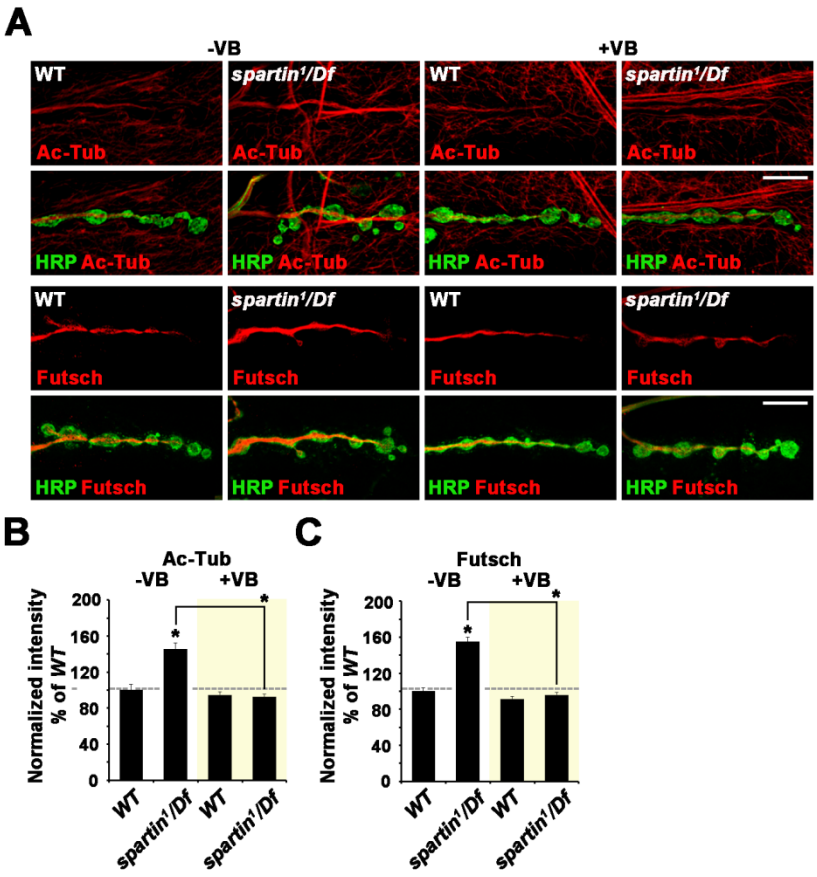
A
-VB
+VB
WT
spartin¹/Df
Ac-Tub
HRP Ac-Tub
Futsch
HRP Futsch
B
Ac-Tub
C
Futsch
Normalized intensity
% of WT
200
160
120
80
40
0
*

Figure 20. Vinblastine, a Microtubule Drug, Suppresses the Accumulation of Acetylated α-Tubulin and Futsch at *spartin* Mutant NMJs

(A) Single confocal images of larval NMJs doubly stained with anti-acetylated α-tubulin or anti-Futsch with anti-HRP shown for wildtype and *spartin*^{1}*/Df* larvae treated in the absence (-VB) or presence (+VB) of 1 μM vinblastine. Scale bars, 10 μm. (B-C) Quantification of the ratio of average acetylated α-tubulin or Futsch to HRP levels in wildtype (WT) and *spartin*^{1}*/Df* larvae. Values represent % of wild-type (*$p < 0.001$).

heterozygous *spartin*^{1}/+, *dad*^{j1e4}/+, or *dfmr1*$^{\Delta 50}$ larvae, overall bouton number and satellite bouton number were wildtype levels **(Figure 21A)**. However, both parameters of synaptic growth were significantly increased in transheterozygous *spartin*^{1}/+; *dfmr1*$^{\Delta 50}$ /+ and *dfmr1*$^{\Delta 50}$ /+; *dad*^{j1e4}/+ larvae compared with any of the single heterozygotes alone **(Figure 21A)**, supporting a role for dFMR1 in Spartin/BMP-mediated regulation of synaptic growth. I next asked whether Spartin and BMP regulate dFMR1 activity through modulation of *dfmr1* expression. Levels of *dfmr1* transcript in the larval CNS (i.e. the brain and the ventral nerve cord) were significantly decreased by loss-of-function mutations of *spartin* or *dad* as well as postsynaptic overexpression of Gbb, while loss-of-function mutations of BMP pathway components had the opposite effect **(Figures 21B)**. Consistently, levels of Futsch protein were similarly affected by the same genetic manipulations **(Figures 22)**. Together, our results argue that both Spartin and BMP regulate synaptic growth by modulating *dfrm1* expression.

9. Loss of *spartin* Function in Neurons Causes Movement Defects and Progressive Neurodegeneration

A clinical hallmark of HSPs is progressive lower limb spasticity and weakness, which severely affects voluntary movement. I therefore examined whether *spartin* mutations in *Drosophila* is also associated with motor dysfunction. I performed a climbing assay for wildtype, control (a precise excision line from the P-element allele G6712) and *spartin* adult flies at 20 days of age. Flies were tapped to the bottom of a graduated cylinder, and the vertical distance climbed by individual flies within 20 s was measured. Compared with control flies, *spartin* mutants displayed significantly reduced climbing ability

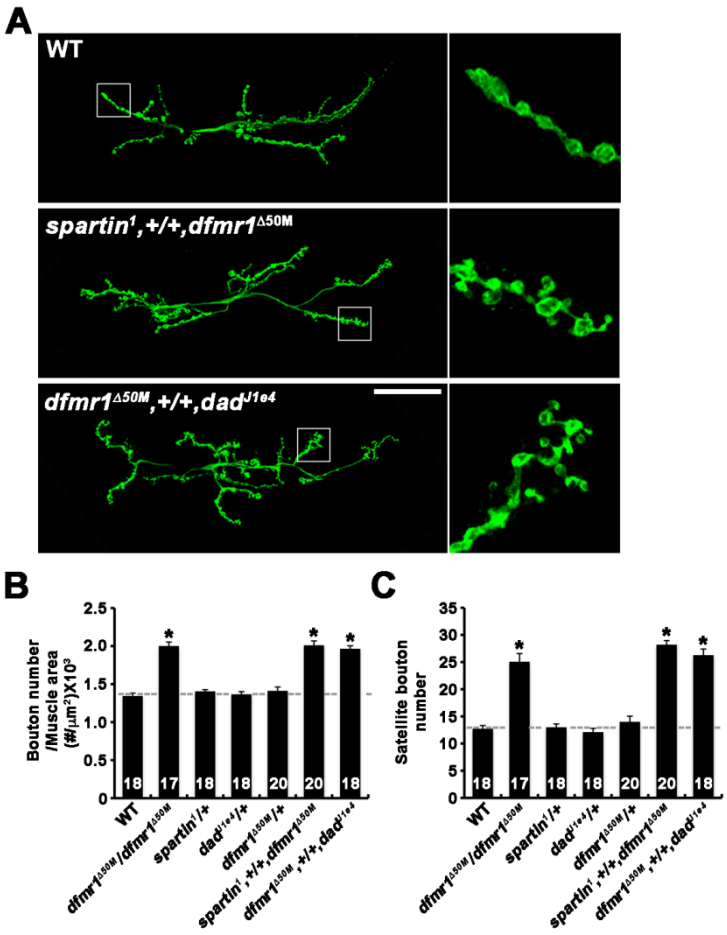
A
WT
spartin1,+/+,dfmr1Δ50M
dfmr1Δ50M,+/+,dadJ1e4
B
Bouton number /Muscle area (#/μm2)X10-3
2.5
2.0
1.5
1.0
0.5
0
18
17
18
18
20
20
18
WT
dfmr1Δ50M/dfmr1Δ50M
spartin1/+
dadJ1e4/+
dfmr1Δ50M/+
spartin1,+/+,dfmr1Δ50M
dfmr1Δ50M,+/+,dadJ1e4
C
Satellite bouton number
35
30
25
20
15
10
5
0
18
17
18
18
20
20
18
WT
dfmr1Δ50M/dfmr1Δ50M
spartin1/+
dadJ1e4/+
dfmr1Δ50M/+
spartin1,+/+,dfmr1Δ50M
dfmr1Δ50M,+/+,dadJ1e4

Figure 21. Transheterozygous Interactions Between *spartin*, *dad* and *dfrmr1*

(A) Confocal images of NMJ 6/7 labeled with anti-HRP shown for wildtype (WT), *dfmr1*$^{\Delta 50M}$/+, *spartin*^{1}, +/+, *dfmr1*$^{\Delta 50M}$ *and dfmr1*$^{\Delta 50M}$, +/+, *dadJLE4* larvae. Scale bar, 50 μm. (B-C) Quantification of overall bouton number normalized to muscle surface area and satellite bouton number at NMJ 6/7 in the following genotypes: wildtype (WT), *dfmr1*$^{\Delta 50M}$/*dfmr1*$^{\Delta 50M}$, *spartin*^{1}/+, *dadJle4/+*, *dfmr1*$^{\Delta 50M}$/+, *spartin*^{1}, +/+, *dfmr1*$^{\Delta 50M}$ *and dfmr1*$^{\Delta 50M}$, +/+, *dadJLE4* larvae (*$p < 0.001$).

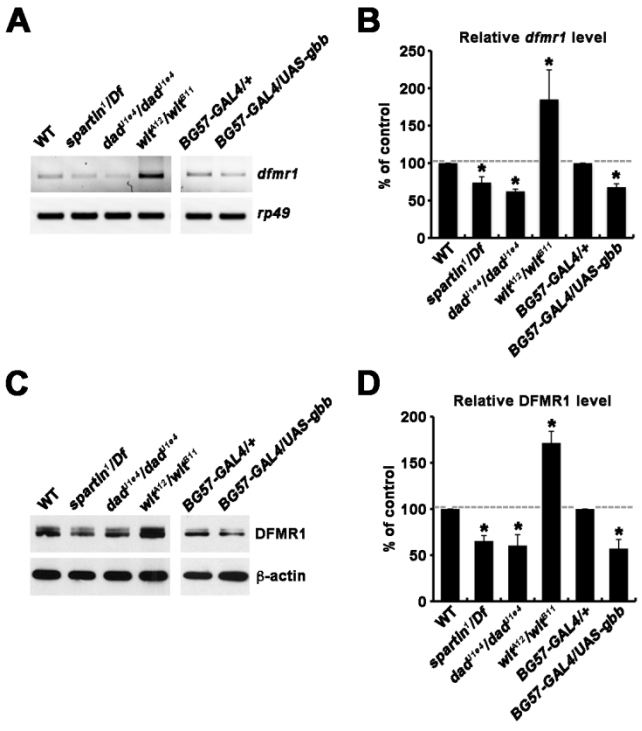
A
WT
spartin1/Df
dad1-4/dad1-4
wit12/wit11
BG57-GAL4/+
BG57-GAL4/UAS-gbb
dfmr1
rp49
B
Relative dfmr1 level
% of control
250
200
150
100
50
0
C
DFMR1
β-actin
D
Relative DFMR1 level

Figure 22. Spartin and BMP Signaling Regulates *dfmr1* Expression in the Larval CNS

(A) RT-PCR analysis of wildtype (WT), *spartin*^{1}*/Df*, *dad*^{Jle4}*/dad*^{Jle4}, *wit*^{A12}*/wit*^{B11}, *BG57-GAL4/+* and *BG-57GAL4/+; UAS-gbb/+* larval CNS using primers specific for *dfmr1* and *rp49*. (B) Quantitation of *dfmr1* RNA expression in the larval CNS using quantitative real-time PCR (qRT-PCR). Samples were run in triplicate in two independent experiments. *rp49* was used as an internal control. (C) Western blot analysis of larval CNS extracts using anti-DFMR1 and anti-β-actin antibodies. (D) Quantitative analysis of the data obtained from three independent experiments by densitometric measurements. β-actin served as an internal control. All comparisons are with wildtype unless indicated (*$p < 0.001$).

(Control: 20 ± 0.5 cm; *spartin*^{1}*/Df*: 20 ± 0.5 cm, $p < 0.001$; **Figures 23A and 23B**). This behavioral phenotype was substantially rescued by either neuronal expression of Spartin or by feeding *spartin* mutants with vinblastine **(Figure 23C)**. In addition, I found that *spartin* mutant regulated lifespan in adult flies. The lifespan was decreased in *spartin*^{1}*/Df* flies compared to revertent and completely rescued by the ubiquitous expression of *spartin* **(Figure 23D)**.

Given a behavioral defect in *spartin* flies, I determined whether loss of Spartin is associated with neurodegeneration, which is manifested by vacuolization in the brain of adult flies (Lee *et al*., 2008). At day 2 after eclosion, *spartin* mutant flies were not significantly different from wildtype controls with respect to anatomical and histological organization of the brain **(Figure 24)**. However, aged *spartin* flies exhibited numerous neuropil vacuoles in the brain. At 10 and 20 days of age, the average number of vacuoles in *spartin* mutants was significantly increased by more than 2.5-fold and 5-fold, respectively, compared with wildtype controls **(Figure 24B)**. The brains of 30- and 40-day-old *spartin* flies exhibited even more vacuolization while age-matched controls were well preserved **(Figure 24B)**. Neurodegeneration defects in *spartin*^{1}*/Df* mutant were completely rescued by presynaptic expression of HA-tagged *Drosophila spartin* (*UAS-HA-spartin*) or Myc-tagged human *spartin* (*UAS-Myc-spartin-human*) form panneuronal driver *C155-GAL4* **(Figures 24C and 24D)**.

To further characterize neurodegeneration in *spartin* mutants, I assessed apoptotic cell death in 20-old brains. While no TUNEL- or caspase-3-positive cells were present in wildtype brains, many nuclei in *spartin* mutant brains were labeled for TUNEL or caspase-3 **(Figures 25)**. The TUNEL- and caspase-3-positive nuclei also labeled with the neuronal marker Elav but not with the glial

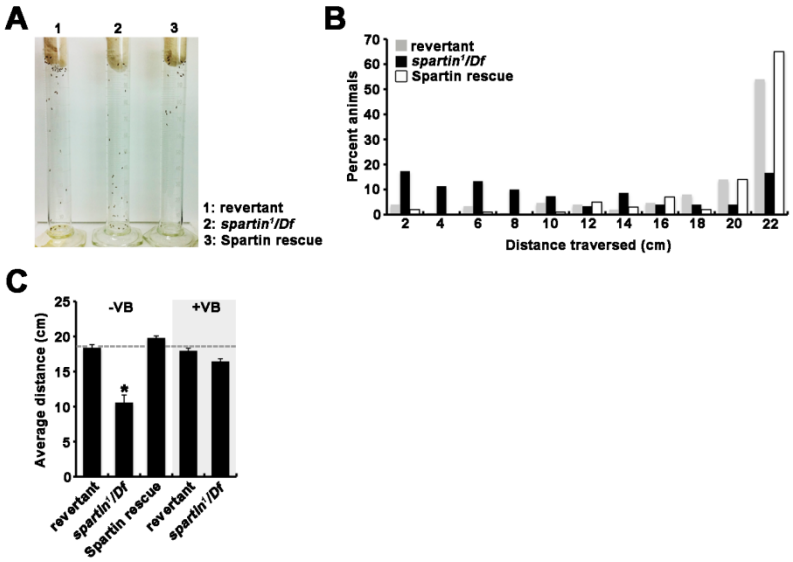
A
1
2
3
1: revertant
2: spartin¹/Df
3: Spartin rescue
B
revertant
spartin¹/Df
Spartin rescue
Percent animals
70
60
50
40
30
20
10
0
2
4
6
8
10
12
14
16
18
20
22
Distance traversed (cm)
C
-VB
+VB
Average distance (cm)
25
20
15
10
5
0
*
revertant
spartin¹/Df
Spartin rescue
revertant
spartin¹/Df

Figure 23. Loss of Neuronal Spartin Severely Impairs Adult Locomotor Activity

(A-B) Distribution of the distance climbed by revertant, *spartin^{1}/Df*, and *C155-GAL4/+*; *Df/UAS-HA-spartin, spartin^{1}* (Spartin rescue) flies measured over 30 sec in a vertical graduated cylinder after the mechanical shock of 10-sec vortexing. (C) Average distance climbed by control and *spartin^{1}/Df* flies grown in the absence (-VB) or presence (+VB) of 1 μM vinblastine. Note that neuronal expression of Spartin or administration of vinblastine improves the locomotor ability of *spartin^{1}/Df* flies to control levels. (D) Survival of female flies under starvation conditions. Genotypes were as follows: revertant, *spartin^{1}/Df* and *Da-GAL4/+; Df/UAS-HA-spartin, spartin^{1}* (Spartin rescue-ubiquitous). The significance of the difference between survival curves (wildtype and *spartin^{1}/Df*) was analyzed. Upon starvation, all *spartin^{1}/Df* strains die at a significantly faster rate as compared to the wildtype flies. (*n*=100 per group).

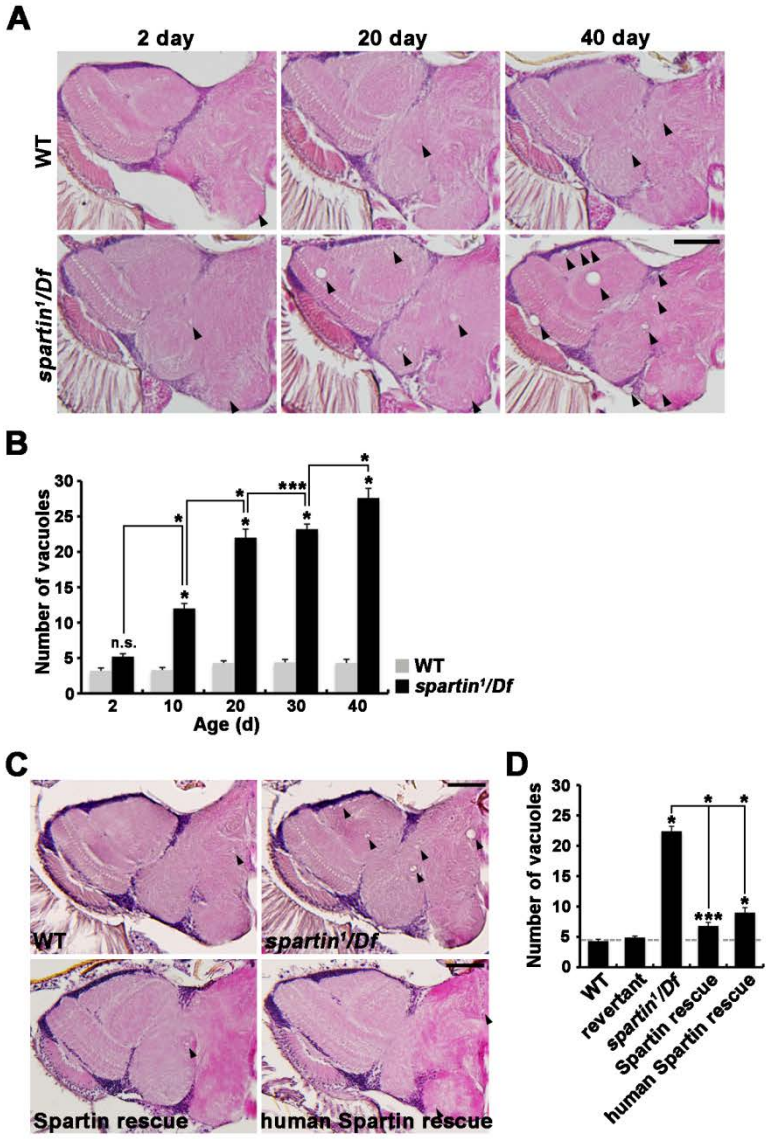
A
2 day
20 day
40 day
WT
spartin¹/Df
B
Number of vacuoles
n.s.
WT
spartin¹/Df
Age (d)
C
WT
spartin¹/Df
Spartin rescue
human Spartin rescue
D
Number of vacuoles
WT
revertant
spartin¹/Df
Spartin rescue
human Spartin rescue

Figure 24. Loss of Spartin Causes Age-Dependent Neurodegeneration

(A) H&E-stained frontal sections (5 μm thick) of brains from 2-day, 10-day, 20-day, 30-day and 40-day-old wildtype (WT) and *spartin*^{1}*/Df* flies. Note that *spartin* brains display increased vacuolization compared with wildtype brains. Vacuoles are marked by black arrows. Scale bars, 50 μm. (B) Quantification of vacuoles with diameter greater than 3 μm in the whole brains of 2-day, 10-day, 20-day, 30-day and 40-day-old wildtype (WT) and *spartin*^{1}*/Df* flies. (C) Representative midline head section of wildtype (WT), *spartin*^{1}*/Df*, Spartin rescue and human Spartin rescue flies stained with H&E staining. Vacuolar degeneration was observed in the cortex and neuropil of *spartin* null mutants. Vacuoles are marked by black arrows. Scale bars: 50 μm. (D) Quantification of vacuoles with diameter greater than 3 μm in the whole brains of 20-day-old wildtype (WT), revertant, *spartin*^{1}*/Df*, *C155-GAL4*, *spartin*^{1}*/UAS-HA-spartin,Df* (Spartin rescue), and *C155-GAL4/+;Df/UAS-HA-human-spartin,spartin*^{1} (human Spartin rescue) flies. All comparisons are with wildtype unless indicated (*$p < 0.001$; ***$p < 0.05$).

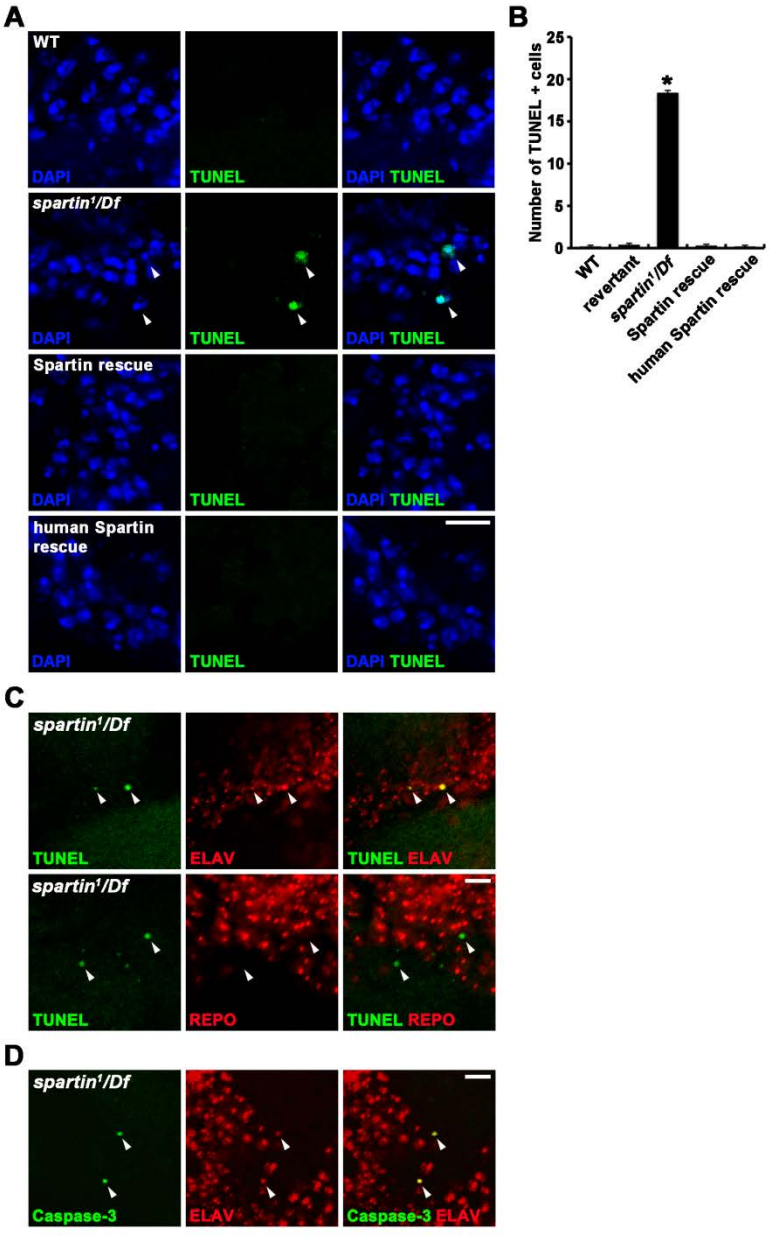
A
WT
DAPI
TUNEL
DAPI TUNEL
spartin¹/Df
DAPI
TUNEL
DAPI TUNEL
Spartin rescue
DAPI
TUNEL
DAPI TUNEL
human Spartin rescue
DAPI
TUNEL
DAPI TUNEL
B
Number of TUNEL + cells
25
20
15
10
5
0
*
WT
revertant
spartin¹/Df
Spartin rescue
human Spartin rescue
C
spartin¹/Df
TUNEL
ELAV
TUNEL ELAV
spartin¹/Df
TUNEL
REPO
TUNEL REPO
D
spartin¹/Df
Caspase-3
ELAV
Caspase-3 ELAV

Figure 25. Programmed Neuronal Cell Death in the *spartin* Mutant Flies
(A) Confocal slices of 20-day-old wildtype (WT), *spartin*^{1}*/Df, C155-GAL4/+; Df/ UAS-spartin, spartin*^{1} (Spartin rescue) and *C155-GAL4/+; Df/ UAS-spartin, spartin*^{1} (human Spartin rescue) adult brain double staining TUNEL and DAPI. Scale bar, 10 μm. (B) Quantification of TUNEL-positive cells (arrows head) observe in three consecutive, middle frontal sections (10 μm thick) form the wildtype, revertant, *spartin*^{1}*/Df*, Spartin rescue and human Spartin rescue. All comparisons are with wildtype unless indicated (*$p < 0.001$). (C-D) A TUNEL-positive or caspase-positive cell expressed the neural marker ELAV, but not the glial marker REPO. Confocal slices of 20-day-old *spartin*^{1}*/Df* brains doubly stained with TUNEL (green) and anti-Elav (red) or anti-Repo (red), or anti-Caspase-3 (green) and anti-Elav (red). Scale bar, 10 μm.

marker Repo **(Figures 25C and 25D)** suggesting that the large majority of cells undergoing apoptosis are neurons. Consistent with this conclusion, neuronal expression of *Drosophila* or human Spartin in *spartin* mutants prevents brain cell death at 20 days of age **(Figure 25D)**.

10. Spartin/BMP-Mediated Regulation of Microtubule Stability Is Critical for Neuronal Survival

Dysregulation of BMP signaling activity has been implicated in various forms of human neurodegenerative diseases including a subset of HSPs (Bayat, *et al*., 2011). To explore the Spartin mechanism preventing neurodegeneration, I assayed phenotypes of *spartin* mutants in BMP signaling and microtubule stability. I found that the levels of Futsch, acetylated α-tubulin and P-Mad were increased in *spartin* adult brain compared to wildtype **(Figures 26A and 26B)**, suggesting that Spartin acts as an inhibitor of BMP signaling. Importantly, most TUNEL- or caspase-3-positive cells in *spartin* mutant brains were strongly labeled for P-Mad **(Figure 26C)**. Therefore, a straight hypothesis is that abnormal elevation of BMP signaling is the major mechanism underlying *spartin*-induced neurodegeneration. To address this issue, I first tested whether abnormal elevation of BMP signaling only in adult neurons could enhance neurodegeneration. For this, animals carrying both *elav-GS-GAL4* and either *UAS- tkv*^{CA} or *UAS-gbb* were fed with the progesterone analog RU486 from right after eclosion and assessed brain vacuolization in 20-day old flies. The number of vacuoles was significantly increased in Tkv^{CA} or Gbb animals compared with the *elav-GS-GAL4* controls **(Figures 27A and 27B)**. Double

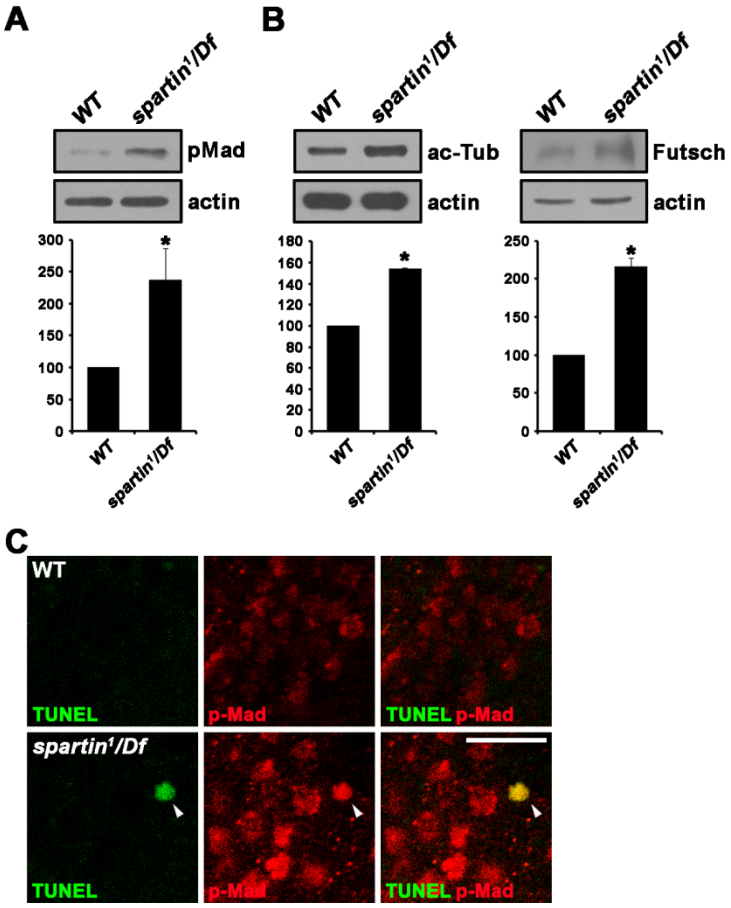
A
WT
spartin¹/Df
pMad
actin
300
250
200
150
100
50
0
*
WT
spartin¹/Df
B
WT
spartin¹/Df
ac-Tub
actin
180
160
140
120
100
80
60
40
20
0
*
WT
spartin¹/Df
WT
spartin¹/Df
Futsch
actin
250
200
150
100
50
0
*
WT
spartin¹/Df
C
WT
TUNEL
p-Mad
TUNEL p-Mad
spartin¹/Df
TUNEL
p-Mad
TUNEL p-Mad

Figure 26. A Loss of *spartin* Increases BMP Signaling Activity and Microtubule Stability in the Adult Brain

(A-B) Western blot analysis of adult brain extracts using antibodies against P-Mad or acetylated α-tubulin or Futsch. Quantitative analysis of the data from three times independent experiments by densitometric measurements. For each sample, the band intensities of P-Mad, acetylated α-tubulin, or Futsch were normalized to that of β-actin. Values shown are the means ± SEM relative to the wildtype control (100%). (C) Confocal slices of 20-day-old wildtype and *spartin*^{1}*/Df* brains doubly stained with TUNEL and anti-P-Mad. Note that P-Mad fluorescence intensity is much higher in *spartin*^{1}*/Df* than in wildtype, and that TUNEL-positive cells display higher P-Mad levels in *spartin* mutants. Scale bar, 10 μm.

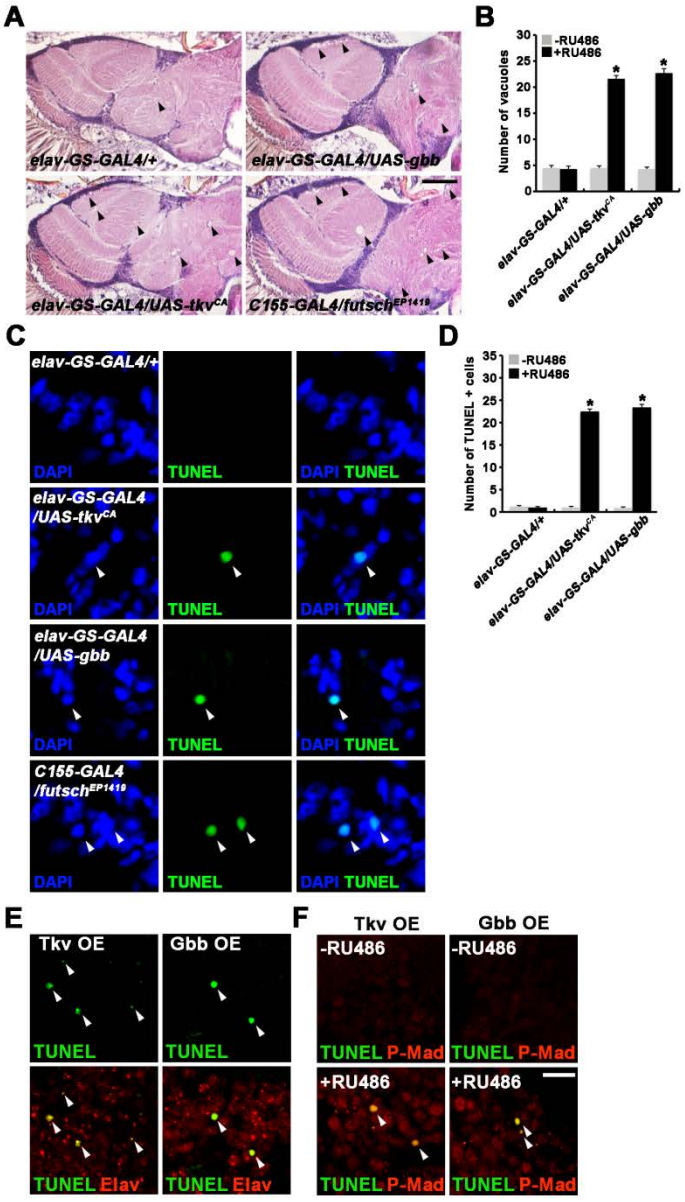
A
elav-GS-GAL4/+
elav-GS-GAL4/UAS-gbb
elav-GS-GAL4/UAS-tkvCA
C155-GAL4/futschEP1419
B
-RU486
+RU486
Number of vacuoles
elav-GS-GAL4/+
elav-GS-GAL4/UAS-tkvCA
elav-GS-GAL4/UAS-gbb
C
elav-GS-GAL4/+
elav-GS-GAL4 /UAS-tkvCA
elav-GS-GAL4 /UAS-gbb
C155-GAL4 /futschEP1419
DAPI
TUNEL
DAPI TUNEL
D
-RU486
+RU486
Number of TUNEL + cells
elav-GS-GAL4/+
elav-GS-GAL4/UAS-tkvCA
elav-GS-GAL4/UAS-gbb
E
Tkv OE
Gbb OE
TUNEL
TUNEL Elav
F
Tkv OE
Gbb OE
-RU486
+RU486
TUNEL P-Mad

Figure 27. Genetic Upregulation of BMP Signaling Causes Neuronal Cell Death in the Adult Brain

(A) H&E-stained frontal sections (5 μm thick) of brains from 20-day-old *elav-GS-GAL4*/*UAS-tkv*^{CA} and *elav-GS-GAL4*/*UAS-gbb* flies. Scale bar, 50 μm. (B) Quantification of vacuoles in the 20-day-old brains of the indicated genotypes. In flies carrying both *elav-GS-GAL4* and either *UAS-tkv*^{CA} or *UAS-gbb* were fed with the progesterone analog RU486 starting right after eclosion. (C) Confocal slices of 20-day-old *elav-GS-GAL4/+*, *elav-GS-GAL4*/*UAS-tkv*^{CA} and *elav-GS-GAL4*/*UAS-gbb* brains doubly stained with TUNEL (green) and DAPI (blue). Scale bars, 10 μm. (D) Quantification of TUNEL-positive cells observed in three consecutive, middle frontal sections (10 μm thick) of 20-day-old brains from the indicated genotypes. (E-F) Confocal slices of 20-day-old *elav-GS-GAL4*/*UAS-tkv*^{CA} (Tkv OE) and *elav-GS-GAL4*/*UAS-gbb* (Gbb OE) flies brains doubly stained with TUNEL (green) and anti-Elav (red) or TUNEL (green) and anti-P-Mad (red). The sample size was $n = 10$ animals for each genotype. All comparisons are with the *elav-GS-GAL4* control unless indicated ($^*p < 0.001$).

staining of UAS-tkvCA or UAS-gbb adult brain with TUNEL and anti-Elav revealed that elevated BMP signaling colocalized with neuronal cell death **(Figure 27)**. Indeed, cell death occurred only in neurons with elevated levels of P-Mad (**Figure 27F**). I then tested whether downregulation of BMP signaling could rescue *spartin* mutant animals with respect to neurodegeneration. Removing one copy of *wit*, which has no effect on brain vacuolization in wildtype, significantly suppressed the vacuolization phenotype of *spartin* mutant brains (**Figure 28**). In addition, I obtained a complete rescue with neuronal overexpression of Dad, which itself caused a significant level of brain vacuolization (**Figure 28**). These data strongly support the model that Spartin acts to maintain neuronal survival by regulating BMP signaling. Finally, I asked if upregulation of Futsch levels and microtubule stability might be responsible for neurodegeneration caused by *spartin* mutations and overactivation of BMP signaling. I obtained the brain degeneration phenotype by overexpressing Futsch only in adult neurons (**Figure 29**). In addition, heterozygosity for $futsch^{k68}$, which has no effect on neurodegeneration in a wildtype background, suppressed the neurodegeneration phenotype associated with *spartin* loss-of-function and enhanced BMP signaling (**Figure 29**)**.** Furthermore, feeding adult flies with vinblastine at a concentration, which had no effect on brain anatomy, ameliorates brain degeneration caused by *spartin* loss-of-function mutations and genetic manipulations enhancing BMP signaling (**Figure 30**). Taken together, these data imply that Spartin/BMP signaling-dependent regulation of Futsch levels and microtubules is critical for maintaining neuronal cell survival in the adult brain.

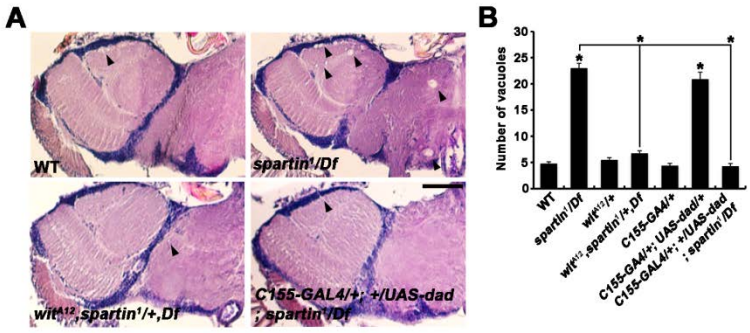

Figure 28. *spartin* Interacts with BMP Pathway Components in the Adult Brain

(A) H&E-stained frontal sections (5 μm thick) of brains from 20-day-old wild-type (WT), *spartin*^{1}*/Df*, *wit*^{A12}, *spartin*^{1}*/+*, *Df* and *C155-GAL4/+; +/UAS-dad; spartin*^{1}*/Df* flies. Vacuoles are marked by black arrows. Scale bar, 50 μm. (B) Quantification of vacuoles in 20-day-old wildtype, *spartin*^{1}*/Df*, *wit*^{A12}*/+*, *wit*^{A12}*,spartin*^{1}*/+,Df*, *C155-GAL4/+*, *C155-GAL4/+;UAS-dad/+*, and *C155-GAL4/+;+/UAS-dad;spartin*^{1}*/Df*. (*$p < 0.001$).

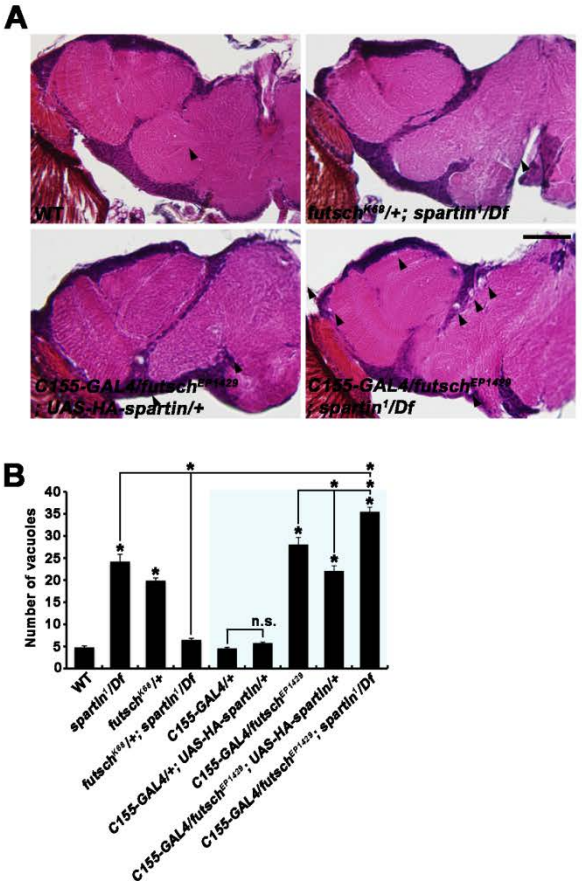
A
WT
futsch^K68/+; spartin^1/Df
C155-GAL4/futsch^EP1429 ; UAS-HA-spartin/+
C155-GAL4/futsch^EP1429 ; spartin^1/Df
B
Number of vacuoles
n.s.
WT
spartin^1/Df
futsch^K68/+
futsch^K68/+; spartin^1/Df
C155-GAL4/+
C155-GAL4/+; UAS-HA-spartin/+
C155-GAL4/futsch^EP1429
C155-GAL4/futsch^EP1429; UAS-HA-spartin/+
C155-GAL4/futsch^EP1429; spartin^1/Df

Figure 29. *spartin* Genetically Interacts with Futsch in the Adult Brain

(A) H&E stained frontal section (5 μm thick) of brains from 20-day-old adult flies. Vacuoles are marked by black arrow. (B) Quantification of vacuoles in the 20-day-old brains from the indicated genotypes from wildtype (WT), *spartin*^{1}*/Df*, *futsch*^{K68}*/+*, *futsch*^{K68}*/+;spartin*^{1}*/Df*, *C155-GAL4/+*, *C155-GAL4/+;UAS-HA-spartin/+*, *C155-GAL4/futsch*^{EP1429}, *C155-GAL4/futsch*^{EP1429}*; UAS-HA-spartin/+* and *C155-GAL4/futsch*^{EP1429}*; spartin*^{1}*/Df*. (**p* < 0.001; n.s., not significant).

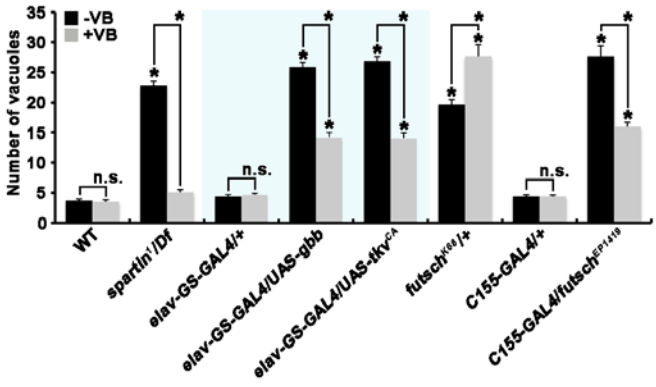

Figure 30. Vinblastine Treatment Ameliorates Vacuolization Induced by *spartin* Mutation or Overactivation of BMP Signaling and Futsch

Quantification of vacuoles in the whole brains of 20-day-old wildtype (WT), *spartin*^{1}*/Df*, *elav-GS-GAL4/+*, *elav-GS-GAL4/UAS-gbb*, *elav-GS-GAL4/UAS-tkv*^{CA}, *futsch*^{K68}*/+*, *C155-GAL4/+* and *C155-GAL4/futsch*^{EP1419} flies in the absence (-VB) or presence (+VB) of 1 μM vinblastine. The sample size was n = 10 animals for each genotype. (*$p < 0.001$; n.s., not significant).

IV. DISCUSSION

Mutations in the human *spartin* gene cause Troyer syndrome, an autosomal recessive form of HSP that is characterized primarily by degeneration of corticospinal tract axons. Previous studies in mammals suggest that the Spartin protein regulates diverse cellular processes, including lipid droplet turnover (Eastman *et al*., 2009), cytokinesis (Renvoise *et al*., 2010), mitochondrial Ca^{2+} homeostasis (Joshi *et al*., 2011), and intracellular EGFR trafficking (Bakowska *et al*., 2007). Despite this progress, the cellular basis for neurodegeneration observed in Troyer syndrome remains largely unclear. Here, I generate a *Drosophila* disease model to investigate the *in vivo* functions of Spartin and to gain insight into the pathogenic mechanism of Troyer syndrome. I provide evidence that Spartin inhibits neuronal BMP signaling by regulating the endocytic internalization of the type II BMP receptor Wit. BMP signaling in turn regulates the dFMR1-Futsch cascade to modulate neuronal microtubule stability, which controls synaptogenesis and neuronal survival. This study is the first demonstration the *in vivo* function of Spartin function in the developing nervous system and suggests a mechanistic basis underlying the neurodegeneration in Troyer syndrome (**Figure 31**).

In cultured mammalian cells, Spartin is transiently associated with membranes of various subcellular organelles, depending on the cell type and the physiological condition. For example, upon EGF stimulation of HeLa cells, Spartin is recruited from the cytoplasm to endosomal structures containing internalized EGFR (Edwards *et al*., 2009; Bakowska *et al*., 2007). When the same cells are treated with oleic acid, Spartin can also localize to the surface of

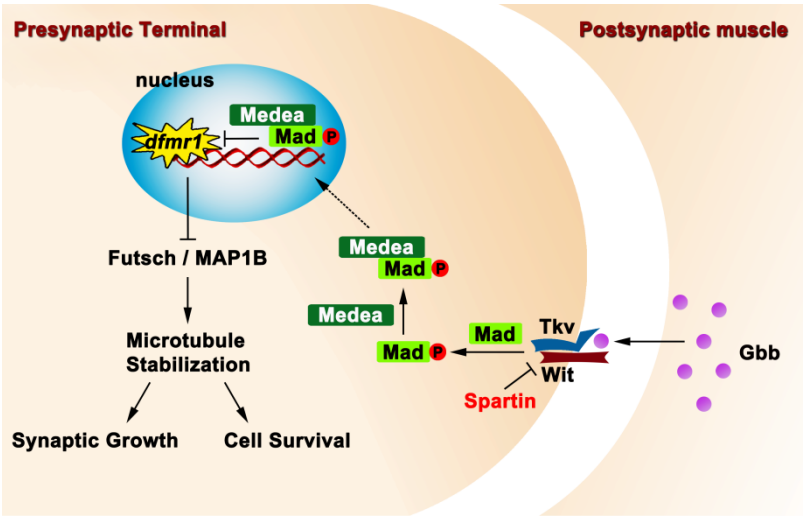

Figure 31. Model for Spartin/BMP Signaling-Dependent Regulation of Synaptic Growth and Neuronal Cell Survival

Retrograde BMP signaling has been demonstrated to promote synaptic growth and neurotransmitter release. In addition, dysregulation of microtubule dynamics leads to axonal transport defects and progressive neurodegeneration in *Drosophila*. I provide evidence that Spartin inhibits neuronal BMP signaling by regulating the endocytic internalization and subsequent endosomal trafficking of the type II BMP receptor Wit. BMP signaling in turn regulates the dFMRP translational regulator controlling Futsch expression to modulate neuronal microtubule stability, which controls both synaptic growth and neuronal survival.

lipid droplets (Eastman *et al*., 2009; Edwards *et al*., 2009). However, in neuroblastoma cells, Spartin is shown to associate with several different organelles: the *trans*-Golgi network, mitochondria, and synaptotagmin-enriched vesicles along neuritis (Robay *et al*., 2006). Nevertheless, the subcellular distribution of mammalian Spartin, particularly in the nervous system, has largely remained unclear. In this study, I show that *Drosophila* Spartin is enriched presynaptically at the NMJ and is mostly associated with periactive zones on the presynaptic membrane, with a small portion localized to presynaptic endosomes. This subcellular distribution is extensively overlapped with that of *Drosophila* Eps15, which acts with Dap160 to control synaptic vesicle endocytosis (Koh *et al*., 2007; Majumdar *et al*., 2006).

Consistent with its strong colocalization with Eps15, Spartin appears to function together with Eps15 at the NMJ synapse. First, loss-of-function *spartin* mutations cause synaptic overgrowth with excessive satellite bouton formation and impairments in FM1-43FX dye uptake. These defects are also observed in *eps15* mutants, suggesting a functional relationship between Spartin and Eps15. Second, *spartin* and *eps15* show transheterozygous interactions during synaptic growth and FM1-43FX uptake, indicating that they function in the same pathway. Finally, the Eps15-binding domain in Spartin is also essential for its synaptic localization. Thus, Spartin is involved in synaptic vesicle endocytosis and synaptic growth regulation through interaction with Eps15.

What is the relationship between the two seemingly unrelated roles for Spartin in synaptic growth and endocytosis regulation? Previous studies at the *Drosophila* NMJ have suggested that abnormal elevation of BMP signaling, which can be achieved by mutations impairing the internalization of surface BMP receptors, causes synaptic overgrowth with excessive satellite bouton

formation (O'Connor-Giles *et al*., 2008; Wang *et al*., 2007). Since satellite bouton formation is also excessive in *spartin* mutants, it was attractive to hypothesize that Spartin restrains synaptic growth by promoting the endocytic downregulation of surface BMP receptors. Our results are consistent with this idea. I show that P-Mad levels at presynaptic termini and in motor neuron nuclei are elevated in *spartin* mutants. In addition, genetic interaction experiments suggest that synaptic overgrowth in *spartin* mutants is dependent on normal BMP signaling. Importantly, I also demonstrate that Spartin promotes the internalization of the type II BMP receptor Wit. Similarly, mammalian Spartin regulates internalization and degradative endosomal sorting of EGFR (Bakowska *et al*., 2007). Our findings thus reveal that the role for Spartin in receptor-mediated endocytosis is conserved between *Drosophila* and mammals. At present, the mechanism of Spartin action in synaptic endocytosis still remains to be determined.

At present, it still remains to be determined how Spartin is involved in endocytosis and endosomal sorting of the BMP receptor Wit? In mammals, endocytosis of EGF receptor can occur through clathrin-dependent and cavelolin-dependent pathways, depending on the concentration of the ligand EGF. Interestingly, the clathrin pathway recycles internalized EGFR to the cell surface for sustained signaling, while the cavelolin pathway targets the receptor to lysosomes for degradation (Sigismund *et al*., 2005). The latter pathway depends on both EGFR ubiquitination by the E3 ubiquitin ligase Cbl and the interactions between ubiquitinated receptor and ubiquitin-interacting motif (UIM)-containing endocytic or endosomal sorting proteins, including Eps15 or hepatocyte growth factor-regulated tyrosine kinase substrate (Hrs), respectively (Sigismund *et al*., 2005). Given these studies, it is worth to note that

mammalian Spartin functions as an adaptor for HECT (homologous to the E6AP carboxyl terminus)-type ubiquitin E3 ligases such as atrophin-interacting protein 4 (AIP4) (Edwards *et al*., 2009; Hooper *et al*., 2010) and that the mammalian, type II BMP receptor (BMPR-II) is constitutively downregulated by AIP4-mediated ubiquitination and subsequent lysosomal degradation[42]. Based on these additional findings, I speculate that Spartin may, through its interactions with AIP4 and Eps15, localize ubiquitination reaction in the vicinity of Eps15-containing molecular complexes at the synaptic membrane and on endosomes, thereby inducing Wit ubiquitination for degradation. An alternative or additional possibility is that the Spartin-Eps15 interaction may itself stabilize additional interactions of Eps15 with ubiquitinated Wit or degradative endosomal sorting complexes, thereby promoting receptor degradation. This second model is based on a previous report that mono-ubiquitination of Eps15 may lead to functional inhibition by forming intermolecular interactions between ubiquitin and the UIM2 in the same molecule (Hoeller *et al*., 2006). The Spartin-Eps15 interaction could achieve this role either by masking the site for mono-ubiquitination or by physically preventing the intramolecular interaction of mono-ubiquitinated Eps15. Thus, it will be of great interest to investigate the role for Spartin in ubiquitination of BMP receptors and Eps15.

Genetic studies at the *Drosophila* NMJ have pointed a direct link between microtubule stability and synaptic growth. Loss of Spastin, a microtubule-severing protein whose human ortholog is mutated in ~40% of autosomal dominant HSP patients, leads to the accumulation of stable microtubules at NMJ presynaptic terminals as well as an increase in the number of overall bouton number and satellite bouton formation (Orso *et al*., 2005;

Sherwood *et al*., 2004). In contrast, loss of Futsch, the *Drosophila* homolog of mammalian microtubule-associated protein 1B (MAP1B), disrupts synaptic microtubule organization and reduces bouton number (Roos *et al*., 2000), further supporting that precise regulation of microtubule stability by microtubule accessory proteins is critical for normal synaptic growth. Because axonal and synaptic levels of Futsch have been shown to be regulated by BMP signaling (Ellis *et al*., 2010), an interesting question arises as to whether Futsch and the microtubule cytoskeleton are major targets for BMP signaling in regulating synaptic growth. Here, I show that synaptic growth defects caused by abnormal elevation of BMP signaling are completely suppressed by additional mutations in *futsch* and treatment of the microtubule-destabilizing agent vinblastine. Based on these observations, I propose that Futsch-dependent regulation of microtubule stability is a major target for BMP signaling in the regulation of synaptic growth.

A role for BMP signaling in the regulation of MAP expression has also been described in mammalian systems. Specifically, BMP2, BMP6, and BMP7 are shown to promote dendrite formation by increasing the expression of microtubule-associated protein-2 (MAP2) in cultured mammalian neurons (Withers *et al*., 2000). However, subsequent work have demonstrated that BMP7 is also able to induce microtubule stabilization by rapidly activating Jun N-terminal kinase (JNK) (Podkowa *et al*., 2010), which in turn regulates microtubule stability through phosphorylation of MAP2 (Björkblom *et al*., 2005). Thus, mammalian BMPs can induce MAP activity via several distinct mechanisms. In *Drosophila* motor axons, the only well-established mechanism of action for BMP signaling is via regulation of Futsch expression. Nevertheless, the mechanism by which BMP signaling regulates Futsch

remains largely unknown. Here, I provide evidence demonstrating that *Drosophila* FMR1 (dFMR1), a known translational repressor of *futsch* mRNA (Zhang *et al*., 2001), acts downstream of Spartin and BMP signaling to modulate Futsch levels in motor axons. Mutations in *dfmr1* displayed transheterozygous interactions with *spartin* or *dad* at the NMJ, suggesting that they act in the same pathway. In addition, the synaptic overgrowth phenotypes of *spartin* and *dad* are completely suppressed by neuronal overexpression of dFMR1, demonstrating that dFMR1 acts downstream of Spartin and BMP pathway components. Furthermore, loss of Spartin or genetic elevation of BMP signaling reduces dFMR1 expression, whereas disruption of BMP signaling by *wit* mutations has the opposite effect. Taken together, our data strongly support the model that dFMR1 mediates the action of Spartin and BMP signaling in regulating Futsch levels. The potential relevance of FMR1 in mediating the effect of BMPs on MAP expression in mammalian systems remains to be determined in the future.

Increasing evidence suggests a potential connection between elevated BMP signaling and a subgroup of HSPs. Specifically, Spichthyin (Spict), the *Drosophila* ortholog of the HSP protein NIPA1, is shown to inhibit BMP signaling by regulating BMP receptor trafficking (Wang *et al*., 2007). Subsequent studies in mammalian cells have confirmed that NIPA1 indeed inhibits BMP signaling by promoting endocytosis and lysosomal degradation of BMP receptors (Tsang *et al*., 2009). Moreover, although the mechanism has remained unknown, other HSP proteins (Atlastin, Spastin, and Spartin) have also been proved as BMP inhibitors in mammalian cells or zebrafish (Fassier *et al*., 2010; Tsang *et al*., 2009), suggesting abnormal elevation of BMP signaling as a common pathologic component of at least several HSPs. However, it has

not been tested whether regulation of BMP signaling by HSP-associated proteins plays a critical role for the maintenance of the adult CNS. Our findings support a causative role for elevated BMP signaling in *spartin*-induced neurodegeneration. First, I observe progressive, age-dependent neurodegeneration in the adult brains of *spartin* nulls. Second, elevation of BMP signaling in a wildtype background, as achieved by expressing either constitutively active Tkv or Gbb, also induces neuronal cell death. Third, neurodegeneration in *spartin* mutants is ameliorated by overexpressing the BMP inhibitor Dad specifically in neurons. These data suggest that neurodegeneration in *spartin* mutants is largely due to elevation of BMP signaling.

A final point of interest relates to the involvement of dysregulated microtubules in neurodegeneration caused by Spartin loss or elevated BMP signaling. I show that neurodegeneration in *spartin* is strongly suppressed by Futsch overexpression, which can itself induce neurodegeneration in the wildtype background. In addition, feeding adult animals with the microtubule-destabilizing drug vinblastine rescues neurodegeneration caused by *spartin* mutations and elevated BMP signaling, respectively. These results support a model in which Spartin/BMP-mediated regulation of microtubule stability via Futsch is critical for the maintenance of the nervous system. Defects in microtubule organization and microtubule-dependent cellular processes (e.g., axonal transport) have been proposed as pathogenic mechanisms of many neurodegenerative diseases, including HSPs (Falnikar and Baas, 2009). However, despite increased levels of stable axonal microtubules, fast axonal transport appears to be normal in *spartin* mutants. Similarly, fast axonal transport is not impaired by loss of Spict, which also negatively regulates BMP-

dependent microtubule organization (Wang *et al*., 2007). Thus, it is an interesting future area for research to investigate how microtubule dysregulation caused by the absence of these HSP-associated proteins induce neurodegeneration in the adult CNS.

V. References

Aberle, H., Haghighi, A.P., Fetter, R.D., McCabe, B.D., Magalhães, T.R. and Goodman, C.S. (2002). wishful thinking encodes a BMP type II receptor that regulates synaptic growth in Drosophila. *Neuron* **33**, 545-558

Adams, M.D., S.E., Celniker, R.A., Holt, C.A., Evans, J.D., Gocayne, P.G. and Amanatides, S.E. (2000). The genome sequence of Drosophila melanogaster. *Science* **287**, 2185-2195

Bakowska, J.C., Jenkins, R., Pendleton, J. and Blackstone, C. (2005). The Troyer syndrome (SPG20) protein spartin interacts with Eps15. *Biochem. Biophys. Res. Commun*. **334**, 1042-1048

Bakowska, J.C., Jupille, H., Fatheddin, P., Puertollano, R. and Blackstone, C. (2007). Troyer syndrome protein spartin is mono-ubiquitinated and functions in EGF receptor trafficking. *Mol Biol Cell* **18**, 1683-1692

Bakowska, J.C., Wang, H., Xin, B., Sumner, C.J. and Blackstone, C. (2008). Lack of spartin protein in Troyer syndrome: a loss-of-function disease mechanism? *Arch Neurol* 65, 520-524

Bayat, V., Jaiswal, M. and Bellen, H.J. (2011). The BMP signaling pathway at the Drosophila neuromuscular junction and its links to neurodegenerative diseases. *Current Opinion in Neurobiology* **21**, 182-188

Bettencourt da Cruz, A., Schwärzel, M., Schulze, S., Niyyati, M., Heisenberq, M. and Kretzschmar, D. (2005). Disruption of the MAP1B-related protein FUTSCH leads to changes in the neuronal cytoskeleton, axonal transport defects, and progressive neurodegeneration in Drosophila. *Mol Biol Cell* **16**, 2433-2442

Blackstone, C., O'Kane, C.J. and Reid, E. (2011). Hereditary spastic paraplegias: membrane traffic and the motor pathway. *Nat. Rev. Neurosci* **12**, 31-42

Björkblom, B., Ostman, N., Hongisto, V., Komarovski, V., Filé, J.J., Nyman, T.A., Kallunki, T., Courtney, M.J. and Coffey, E.T. (2005). Constitutively active cytoplasmic c-Jun N-terminal kinase 1 is a dominant regulator of dendritic architecture: role of microtubule-associated protein 2 as an effector. *J. Neurosci*. **25**, 6350-6361

Ciccarelli, F.D., Proukakis, C., Patel, H., Cross, H., Azam, S., Patton, M.A., Bork, P. and Crosby, A.H. (2003). The identification of a conserved domain in both spartin and spastin, mutated in hereditary spastic paraplegia. *Genomics*. **81**, 437-441.

Coffee, R.L., Jr., Tessier, C.R., Woodruff, E.A., 3rd, and Broadie, K. (2010). Fragile X mental retardation protein has a unique, evolutionarily conserved neuronal function not shared with FXR1P or FXR2P. *Dis. Model Mech*. **3**, 471-485.

Cross, H.E. and McKusick, V.A. (1967). The Troyer syndrome. A recessive form of spastic paraplegia with distal muscle wasting. *Arch. Neurol*. **16**, 473-485

Eastman, S.W., Yassaee, M. and Bieniasz, P.D. (2009). A role for ubiquitin ligases and Spartin/SPG20 in lipid droplet turnover. *J. Cell Biol*. **184**, 881-894

Edwards, T.L., Clowes, V.E., Tsang, H.T., Connell, J.W., Sanderson, C.M., Luzio, J.P. and Reid, E. (2009). Endogenous spartin (SPG20) is recruited to endosomes and lipid droplets and interacts with the ubiquitin E3 ligases AIP4 and AIP5. *Biochem. J*. **423**, 31-39

Ellis, J.E., Parker, L., Cho, J. and Arora, K. (2010). Activin signaling functions upstream of Gbb to regulate synaptic growth at the Drosophila neuromuscular junction. *Dev Biol* **342**, 121-133.

Falnikar, A., and Baas, P.W. (2009). Critical roles for microtubules in axonal development and diseases. *Results Probl. Cell Differ*. **48**, 47-64

Fassier, C., Hutt, J.A., Scholpp, S., Lumsden, A., Giros, B., Nothias, F., Schneider-Maunoury, S., Houart, C. and Hazan, J., (2010). Zebrafish atlastin controls motility and spinal motor axon architecture via inhibition of the BMP pathway. *Nat. Neurosci.* **13**, 1380-1387

Fink, J.K. (2003). Advances in the hereditary spastic paraplegias. *Exp. Neurol*. **184**, S106-110

Goold, R.G., Owen, R. and Gordon-Weeks, P.R. (1999). Glycogen synthase kinase 3beta phosphorylation of microtubule-associated protein 1B regulates the stability of microtubules in growth cones. *J Cell Sci* **112 (Pt 19)**, 3373-3384

Harding, A.E. (1983). Classification of the hereditary ataxias and paraplegias. *Lancet*. **1**, 1151-1155

Hoeller, D., Crosetto, N., Blagoev, B., Raiborg, C., Tikkanen, R., Wagner, S., Kowanetz, K., Breitling, R., Mann, M., Stenmark, H. and Dikic, I. (2006). Regulation of ubiquitin-binding proteins by monoubiquitination. *Nat Cell Biol* **8**, 163-169

Hooper, C., Puttamadappa, S.S., Loring, Z., Shekhtman, A. and Bakowska, J.C. (2010). Spartin activates atrophin-1-interacting protein 4 (AIP4) E3 ubiquitin ligase and promotes ubiquitination of adipophilin on lipid droplets. *BMC Biol.* **8**, 72

Joshi, D.C. and Bakowska, J.C. (2011). SPG20 protein Spartin associates with cardiolipin via lts plant-related senescence domain and regulates mitochondrial Ca2+ homeostasis. *PLoS ONE* **6(4)**, e19290

Kalinovsky, A. and Scheiffele, P. (2004). Transcriptional control of synaptic differentiation by retrograde signals. *Curr Opin Neurobiol* **14**, 272-279

Kim, S., Wairkar, Y.P., Daniels, R.W. and DiAntonio, A. (2010). The novel endosomal membrane protein Ema interacts with the class C Vps-HOPS complex to promote endosomal maturation. *J Cell Biol* **188**, 717-734

Koh, T.W., Korolchuk, V.L., Wairkar, Y.P., Jiao, W., Evergren, E., Pan, H., Zhou, Y., Venken, K.J., Shupliakov, O., Robinson, I.M., O'Kane, C.J. and Bellen, H.J. (2007). Eps15 and Dap160 control synaptic vesicle membrane retrieval and synapse development. *J Cell Biol* **178**, 309-322

Lee, Y., Paik, D., Bang, S., Kang, J., Chun, B., Lee, S., Bae, E., Chung, J. and Kim, J. (2008). Loss of spastic paraplegia gene atlastin induces age-dependent death of dopaminergic neurons in Drosophila. *Neurobiol Aging* **29**, 84-94

Majumdar, A., Ramagiri, S. and Rikhy, R. (2006). Drosophila homologue of Eps15 is essential for synaptic vesicle recycling. *Exp Cell Res* **312**, 2288-2298

Manzini, M.C., Rajab, A., Maynard, T.M., Mochida, G.H., Tan, W.H., Nasir, R., Hill, R.S., Gleason, D., Al Saffar, M., Partlow, J.N., Barry, B.J., Vernon, M., LaMantia, A.S. and Walsh, C.A. (2010). Developmental and degenerative features in a complicated spastic paraplegia. *Ann. Neurol*. **67**, 516-525

Marques, G. and Zhang, B. (2006). Retrograde signaling that regulates synaptic development and function at the Drosophila neuromuscular junction. *Int Rev Neurobiol* **75**, 267-285

Marques, G., Bao, H., Haerry, T.E., Shimell, M.J., Duchek, P., Zhang, B. and O'Connor, M.B. (2002). The Drosophila BMP type II receptor Wishful

Thinking regulates neuromuscular synapse morphology and function. *Neuron* **33**, 529-543

McCabe, B.D., Marques, G., Haghighi, A.P., Fetter, R.D., Crotty, M.L., Haerry, T.E., Goodman, C.S., and O'Connor, M.B. (2003). The BMP homolog Gbb provides a retrograde signal that regulates synaptic growth at the Drosophila neuromuscular junction. *Neuron* **39**, 241-254.

McCabe, B.D., Hom, S., Aberle, H., Fetter, R.D., Marques, G., Haerry, T.E., Wan, H., O'Connor, M.B., Goodman, C.S. and Haqhiqhi, A.P. (2004). Highwire regulates presynaptic BMP signaling essential for synaptic growth. *Neuron* **41**, 891-905

Mockett, R.J., Radyuk, S.N., Benes, J.J., Orr, W.C. and Sohal, R.S. (2003). Phenotypic effects of familial amyotrophic lateral sclerosis mutant sod alleles in transgenic drosophila, *Proceedings of the National Academy of Sciences of the United States of America* **100**, 301-306

Nahm, M., Kim, S., Pail, S.K., Lee, M., Lee, S., Lee, Z.H., Kim, J., Lee, D., Bae, Y.C. and Lee, S. (2010-a). dCIP4 (Drosophila Cdc42-interacting protein 4) restrains synaptic growth by inhibiting the secretion of the retrograde Glass bottom boat signal. *J Neurosci* **30**, 8138-8150

Nahm, M., Long, A.A., Paik, S.K., Kim, S., Bae, Y.C., Broadie, K. and Lee, S. (2010-b). The Cdc42-selective GAP rich regulates postsynaptic development and retrograde BMP transsynaptic signaling. *J Cell Biol* **191**, 661-675.

Nahm, M., Lee, M., Parkinson, W., Lee, M., Kim, H., Kim, YJ., Kim, S., Cho, YS., Min, BM., Bae, YC., Broadie, K., and Lee, S. (2013). Neuron, *77*, 680-695

O'Connor-Giles, K.M., Ho, L.L. and Ganetzky, B. (2008). Nervous wreck interacts with thickveins and the endocytic machinery to attenuate retrograde BMP signaling during synaptic growth. Neuron *58*, 507-518

Patel, H., Cross, H., Proukakis, C., Hershberger, R., Bork, P., Ciccarelli, F.D., Patton, M.A., McKusick, V.A. and Crosby, A.H. (2002). SPG20 is mutated in Troyer syndrome, an hereditary spastic paraplegia. *Nat. Genet*. **31**, 347-348

Podkowa, M., Zhao, X., Chow, C.W., Coffey, E.T., Davis, R.J. and Attisano, L. (2010). Microtubule stabilization by bone morphogenetic protein receptor mediated scaffolding of c-Jun N-terminal kinase promotes dendrite formation. *Mol. Cell. Biol*. **30**, 2241-2250

Rawson, J.M., Lee, M., Kennedy, E.L. and Selleck, S.B. (2003). Drosophila neuromuscular synapse assembly and function require the TGF-beta type I receptor saxophone and the transcription factor Mad. *J. Neurobiol*. **55**, 134-150

Reid, E., Kloos, M., Ashley-Koch, A., Hughes, L., Bevan, S., Svenson, I.K., Grahanm, F.L., Gaskell, P.C., Dearlove, A., Pericak-Vance, M.A., Rubinsztein, D.C. and Marchuk, D.A. (2002). A kinesin heavy chain (KIF5A) mutation in hereditary spastic paraplegia (SPG10). *Am J. Hum. Genet.* **71**, 1189-1194

Regehr, W.G., Carey, M.R. and Best, A.R. (2009). Activity-dependent regulation of synapses by retrograde messengers. *Neuron* **63**, 154-170.

Renvoise, B., Parker, R.L., Yang, D., Bakowska, J.C., Hurley, J.H. and Blackstone, C. (2010). SPG20 protein spartin is recruited to midbodies by ESCRT-III protein Ist1 and participates in cytokinesis. *Mol Biol Cell* **21**, 3293-3303.

Robay, D., Patel, H., Simpson, M.A., Brown, N.A. and Crosby, A.H. (2006). Endogenous spartin, mutated in hereditary spastic paraplegia, has a complex subcellular localization suggesting diverse roles in neurons. *Exp Cell Res* **312**, 2764-2777.

Roos, J., Hummel, T., Ng, N., Klambt, C. and Davis, G.W. (2000). Drosophila Futsch regulates synaptic microtubule organization and is necessary for synaptic growth. *Neuron.* **26**, 371-382

Rubin, G.M., Yandell, M.D., Wortman, J.R., Gabor Miklos, G.L., Nelson, C.R., Hariharan, I.K., Fortini, M.E., Li, P.W., Apweiler, R., Fleischmann, W., Cherry, J.M., Henikoff, S., Skupski, M.P., Misra, S., Ashburner, M., Birney, E., Boguski, M.S., Brody, T., Brokstein, P., Celniker, S.E., Chervitz, S.A., Coates, D., Cravchik, A., Gabrielian, A., Galle, R.F., Gelbart, W.M., George, R.A., Goldstein, L.S., Gong, F., Guan, P., Harris, N.L., Hay, B.A., Hoskins, R.A., Li, J., Li, Z., Hynes, R.O., Jones, S.J., Kuehl, P.M., Lemaitre, B., Littleton, J.T., Morrison, D.K., Mungall, C., O'Farrell, P.H., Pickeral, O.K., Shue, C., Vosshall, L.B., Zhang, J., Zhao, Q., Zheng, X.H. and Lewis, S. (2000). Comparative genomics of the eukaryotes. *Science* **287**, 2204-2215

Ruiz-Canada, C. and Budnik, V. (2006). Introduction on the use of the Drosophila embryonic/larval neuromuscular junction as a model system to study synapse development and function, and a brief summary of pathfinding and target recognition. *Int Rev Neurobiol* **75**, 1-31.

Schuster, C.M., Davis, G.W., Fetter, R.D. and Goodman, C.S. (1996). Genetic dissection of structural and functional components of synaptic plasticity. I. Fasciclin II controls synaptic stabilization and growth. *Neuron* **17**, 641-654

Sigismund, S., Woelk, T., Puri, C., Maspero, EL, Tacchetti, C., Transidico, P., Di Fiore, P.P. and Polo, S. (2005). Clathrin-independent endocytosis of ubiquitinated cargos. *Proc Natl Acad Sci USA* **102**, 2760-2765.

Simon, A.F., D.T. Liang and D.E. Krantz. (2006). Differential decline in behavioral performance of Drosophila melanogaster with age. *Mechanisms of Ageing and Development* **127**, 647-651

Soderblom, C. and Blackstone, C. (2006). Traffic accidents: Molecular genetic insights into the pathogenesis of the hereditary spastic paraplegias. *Pharmacol. Ther*. **109**, 42-56

Sweeney, S.T. and Davis, G.W. (2002). Unrestricted synaptic growth in spinster-a late endosomal protein implicated in TGF-beta-mediated synaptic growth regulation. Neuron *36*, 403-416.

Tao, H.W. and Poo, M. (2001). Retrograde signaling at central synapses. *Proc Natl Acad Sci U S A* **98**, 11009-11015.

Tsang, H.T., Edwards, T.L., Wang, X., Connell, J.W., Davies, R.J., Durrington, H.J., O'Kane, C.J., Luzio, J.P. and Reid, E. (2009). The hereditary spastic paraplegia proteins NIPA1, spastin and spartin are inhibitors of mammalian BMP signaling. *Hum. Mol. Genet*. **18**, 3805-3821

Urbanczyk, A. and Enz, R. (2011). Spartin recruits PKC-zeta via the PKC-zeta-interacting proteins ZIP1 and ZIP3 to lipid droplets. *J Neurochem* **118**, 737-748.

Vadlamudi, R.K., Barnes, C.J., Rayala, S., Li, F., Balasenthil, S., Marcus, S., Goodson, H.V., Sahin, A.A., Kumar, R. (2005). p21-activated kinase 1 regulates microtubule dynamics by phosphorylating tubulin cofactor B. *Mol Cell Biol* **25**, 3726-3736

Wang, X., Shaw, W.R., Tsang, H.T., Reid, E. and O'Kane, C.J. (2007). Drosophila spichthyin inhibits BMP signaling and regulates synaptic growth and axonal microtubules. *Nat. Neurosci.* **10**, 177-185.

Webster, D.R. and Borisy, G.G. (1989). Microtubules are acetylated in domains that turn over slowly. *J Cell Sci* **92 (Pt 1)**, 57-65

Withers, G.S., Higgins, D., Charette, M. and Banker, G. (2000). Bone morphogenetic protein-7 enhances dendritic growth and receptivity to innervation in cultured hippocampal neurons. *Eur. J. Neurosci.* **12**, 106-116

Yoshihara, M., Ensminger, A.W. and J.T. Littleton. (2001). Neurobiology and the Drosophila genome. *Functional & Integrative Genomics 1* **4**, 235-240

Zhang, Y.Q., Bailey, A.M., Matthies, H.J., Renden, R.B., Smith, M.A., Speese, S.D., Rubin, G.M. and Broadie, K. (2001). Drosophila fragile X-related gene regulates the MAP1B homolog Futsch to control synaptic structure and function. *Cell* **107**, 591-603

Zweifel, L.S., Kuruvilla, R. and Ginty, D.D. (2005). Functions and mechanisms of retrograde neurotrophin signaling. *Nat Rev Neurosci* **6**, 615-625.

국문 초록

Troyer 증후군은 complicated HSP의 한 종류로써, 지금까지 Troyer 증후군과 관련된 원인 유전자는 *spartin* (*SPG20*)이 밝혀져 있다. 본 연구는 초파리를 동물 모델로 이용하여, Spartin의 시냅스 전 말단에서의 기능과 Troyer 증후군의 병리기전을 규명하였다.

Spartin은 시냅스 막과 early endosome에서 특이적으로 발현되며, endocytic adaptor 단백질인 Eps15와 상호작용을 통해 시냅스 성장과 기능을 조절함을 밝혔다. Spartin은 시냅스 전 말단에 존재하는 BMP 수용체인 Wishful Thinking (Wit)의 endocytic degradation을 유도하여 BMP 신호전달을 억제함으로써 시냅스 성장을 저해하며, 이러한 Spartin/BMP 신호전달은 *Drosophila* fragile X mental retardation protein (dFMRP)-Futsch 신호전달과정을 통하여 미세소관의 안정성을 유도함으로써 시냅스 성장을 억제함을 규명하였다. 시냅스의 기능과 더불어 *spartin*의 결손과 BMP 신호전달의 과도한 활성은 HSP 환자들에서 보고된 age-dependent한 운동장애가 관찰되었다. 또한 돌연변이 성체 뇌에서 neurodegeneration에 의한 vacuole 형성이 확인되었으며 이러한 vacuole 형성은 신경세포의 사멸에 의해 유도됨을 규명하였다. 특히 *spartin* 돌연변이에서 관찰된 시냅스의 과 성장과 성체 뇌의 neurodegeneration에 의한 이상은 미세소관의 안정성을 저해하는 약물인 Vinblastine (VB)에 의해 모두 회복됨을 관찰하였다. Spartin이 BMP-dFMRP-Futsch 신호전달을 억제하여 미세소관 안정성을 조절하며, 이를 통해 시냅스 성장과 신경 세포 사멸을 억제함를 밝힌 본 연구는

미세소관의 비정상적인 안정성 조절이 Troyer 증후군이 유발되는 핵심기전임을 제시한다.

주요어: Hereditary spastic paraplegia, Troyer 증후군, Spartin, 미세소관 안전성, BMP 신호전달, 시냅스

학 번: 2008-30635